

USING LATTICE QUANTUM CHROMODYNAMICS FOR
NON-PERTURBATIVE RENORMALIZATION AND CALCULATING
ELECTROMAGNETIC FORM FACTORS OF HYPERONS

By

Matthew David Zeilbeck

A THESIS

Submitted to
Michigan State University
in partial fulfillment of the requirements
for the degree of

Physics—Master of Science

2023

ABSTRACT

Lattice quantum chromodynamics, often abbreviated as lattice QCD or LQCD, presents a non-perturbative method for calculating phenomenological quantities in quantum field theory (QFT). However, scale-dependent quantities such as the gluon momentum fraction $\langle x \rangle_g$ must be renormalized in order to compare lattice calculations to other theory and even other lattice calculations. I obtain the energy spectrum and ground state matrix elements of the gluon energy-momentum tensor (EMT) from the 2pt and 3pt correlators calculated from LQCD. I calculate of the NPR renormalization constants using the regularization-independent momentum subtraction scheme (RI/MOM) for various lattice spacings with a pion mass $M_\pi \approx 310$ MeV. This calculation required various steps in **Chroma** and **Mathematica**, and the workflow for this process is comprehensively detailed. On a different set of lattice ensembles, I utilize the ground state matrix elements of the vector current operator of various quarks, calculated from the 2pt and 3pt correlators, to calculate the Sachs electromagnetic form factors of the nucleon and the Σ and Ξ hyperons. Then I utilize the z -expansion and extract the electric radius $\langle r_E^2 \rangle$ and magnetic radius $\langle r_M^2 \rangle$ as well as the magnetic moment μ of these spin-1/2 baryons.

TABLE OF CONTENTS

Chapter 1	Introduction	1
1.1	Particle Physics	1
1.1.1	Hyperons	3
1.2	The Path Integral Formulation of Quantum Mechanics	5
1.2.1	The Schrödinger Equation, Operator Formalism	5
1.2.2	Feynman’s Path Integral Approach	6
1.2.3	Euclidean Time	7
1.2.3.1	Quantum Mechanics in Euclidean Time	8
1.3	Quantum Field Theory	10
Chapter 2	Quantum Chromodynamics on the Lattice	12
2.1	Continuum QCD	12
2.1.1	The QCD Lagrangian, Gauge Fields, and Color Components	12
2.1.2	Local Gauge Invariance	14
2.2	QCD Actions on the Lattice	14
2.2.1	Lattice Gauge Invariance and Link Variables	15
2.2.1.1	Fermionic Part	15
2.2.1.2	Gauge Part	17
2.3	Evaluating Lattice Quantities	19
2.3.1	Calculating Lattice Quantities	19
2.3.2	Spectral Decomposition of Lattice Quantities	21
Chapter 3	Analyzing Lattice Correlator Data	23
3.1	The 2pt and 3pt Correlators	23
3.1.1	Fitting the 2pt Correlator	25
3.1.2	Fitting the 3pt Correlator	28
Chapter 4	Nonperturbative Renormalization (NPR)	34
4.1	Regularization-independent Momentum Subtraction (RI/MOM) Scheme	34
4.2	Cluster-decomposition Error Reduction (CDER)	37
4.3	Renormalized Gluon Momentum Fraction	39
4.4	NPR Calculation Workflow	42
4.4.1	Chroma	42
4.4.1.1	Implementation of the NPR Calculation	48
4.4.2	Mathematica	49
Chapter 5	Electromagnetic Form Factors	54
Chapter 6	Conclusion	55
	REFERENCES	56

Chapter 1

Introduction

1.1 Particle Physics

All matter in the universe is comprised of particles called leptons and hadrons. Leptons have no further internal composite structure — they are fundamental — while hadrons are made of quarks and are thus composite particles. Hadrons are further classified into mesons and baryons. Mesons are lighter and are made of a quark-antiquark pair while baryons are heavier and made of three quarks. In order for quarks to bind together to make a hadron, they must interact with each other and form a bound state. The nature of these interactions is quite complicated. For example, a proton has three *valence* quarks (up, up, down or *uud*) that are always detectable, but inside the proton, there is a complicated web of interactions involving gluons and virtual quark-antiquark pairs that affect the nature of the proton, see. Fig. 1.1. It used to be believed that the properties of baryons like the proton were almost entirely determined by their valence quarks . However, we now know that this is not the case; it is as a result of both the properties of quarks and the nature of the interactions between them that hadrons acquire various physical properties such as spin, magnetic moment, observable mass¹, effective size, etc.

¹The masses of hadrons like the proton and neutron are not simply the sums of the bare masses of their quarks. Rather, their masses are affected by the complex internal interactions with gluons. It is primarily the energy of the interactions with gluons that we observe as the baryon's mass.

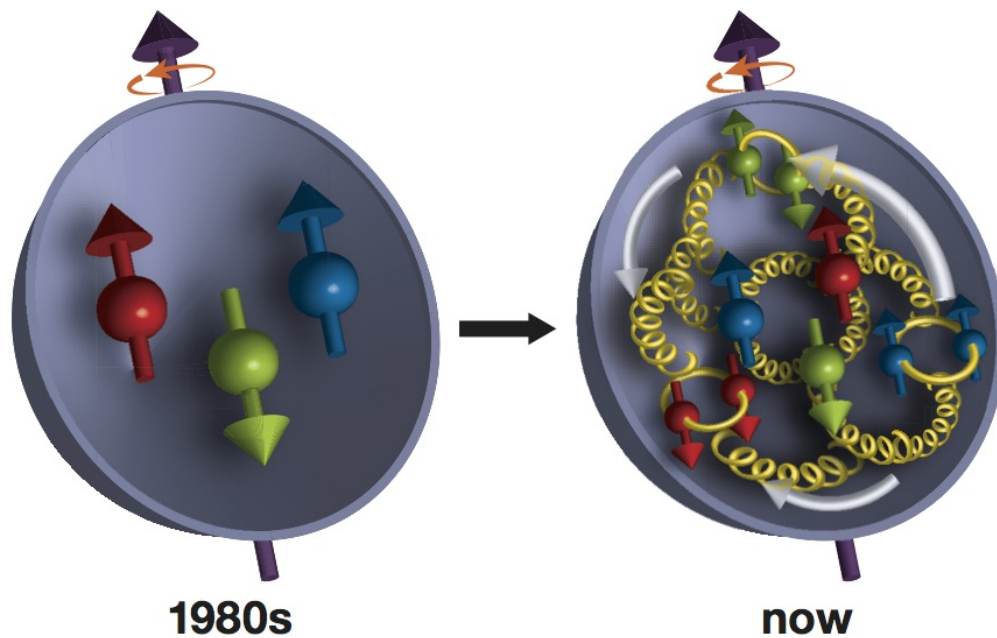


Figure 1.1: Comparison of our understanding of the proton. The left image shows the previous model of the proton as consisting only of its valence quarks since gluon effects were not thought to be important. The right image shows the current understanding of the dynamics of the proton with valence quarks, virtual quarks, and gluons. The larger spheres that represent the valence quarks are made larger for emphasis and do not reflect the relative sizes of particles. The coil-like lines represent gluons that interact with the quarks to which they are attached. Image source [1].

1.1.1 Hyperons

Hyperons are baryons comprised of up, down, and strange quarks with spin-1/2. In terms of Murray Gell-Mann's eightfold way, they represent the strange particles in the baryon octet, see Fig. 1.2. Since hyperons have at least one strange quark, they are heavier than the nucleon which only contains the comparatively extremely light up and down quarks. This makes hyperons unstable as heavier particles have a tendency to decay into lighter particles. This instability leads to problems for experimentalists who want to perform precise experiments with them. Particle physics experiments typically involve accelerating a particle like a proton to nearly the speed of light c and then colliding it into another particle that might also be nearly at c . As long as a collider exists, such as the Large Hadron Collider (LHC) at CERN, and there are energy sources to accelerate the particles, this is not a problem because the proton is stable. Such experiments can provide information about properties of the proton. The task becomes more complicated if we desire to probe out the properties of unstable particles. We cannot accelerate a hyperon and collide it with another particle because it will decay before becoming suitable for collision. Therefore, information about these unstable particles is limited to their creation in hadronic showers after stable particles like protons collide. Since we do not have precise control of the particles in hadronic showers, unlike the particles in a collision, it is difficult to obtain precise measurements of the properties of these particles. This is where lattice quantum chromodynamics (lattice QCD or LQCD) can provide a solution.

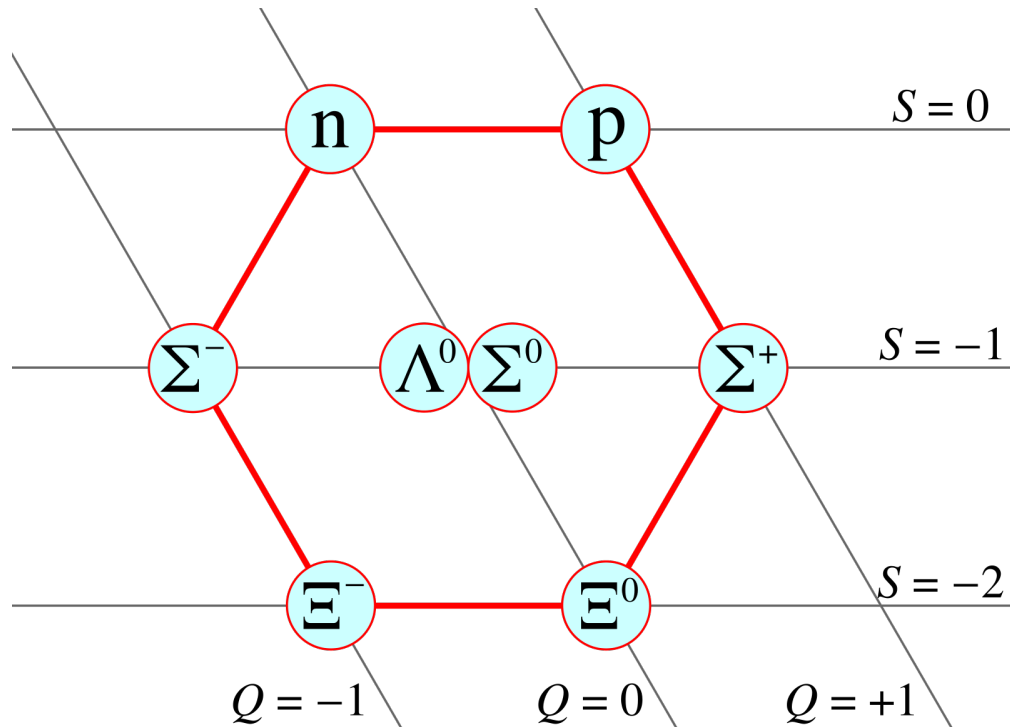


Figure 1.2: The baryon octet of Murray Gell-Mann's eightfold way. This diagram shows all the baryons with spin-1/2 that can be made from up, down, and strange quarks. Particles are arranged such that each row has the same strangeness S and each left-slanted diagonal has the same charge Q (in units of elementary charge). The top row ($S = 0$) contains the nucleons and the bottom two rows ($S = -1, -2$) contain the hyperons. Figure taken from https://commons.wikimedia.org/wiki/File:Baryon_octet.svg.

1.2 The Path Integral Formulation of Quantum Mechanics

1.2.1 The Schrödinger Equation, Operator Formalism

Lattice QCD developed from quantum field theory, which itself was developed from quantum mechanics. In non-relativistic quantum mechanics, one can solve physical problems by obtaining the wavefunction of a system which obeys the Schrödinger equation

$$\left(- \sum_{i=1}^N \frac{\hbar^2}{2m_i} \nabla_i^2 + V(\mathbf{x}_i, t) \right) \Psi(\mathbf{x}_i, t) = i\hbar \frac{\partial}{\partial t} \Psi(\mathbf{x}_i, t), \quad (1.1)$$

where m_i is the mass of the i th particle, $V(\mathbf{x}_i, t)$ is the potential, $\Psi(\mathbf{x}_i, t)$ is the wavefunction, and the sum is over N particles. \mathbf{x}_i is shorthand for the positions of each of the N particles $\{\mathbf{x}_i\}$. However, the wavefunction is overlap of the time-dependent state $|\Psi(t)\rangle$ with the position eigenstate $\langle \mathbf{x}_i|$ such that $\Psi(\mathbf{x}_i, t) = \langle \mathbf{x}_i | \Psi(t) \rangle$. Then we evaluate expectation values of physical quantities with

$$\langle O \rangle (t) = \langle \Psi(t) | \hat{O}(\hat{\mathbf{x}}, \hat{\mathbf{p}}) | \Psi(t) \rangle = \int \Psi^*(\mathbf{x}, t) O(\mathbf{x}, -i\hbar \nabla) \Psi(\mathbf{x}, t) d^3x \quad (1.2)$$

where $\hat{O}(\hat{x}, \hat{p})$ is the operator associated with the observable $\langle O \rangle$ and the hat is used to denote an operator. All operators are functions of the canonical variables $(\hat{\mathbf{x}}, \hat{\mathbf{p}})$ in operator form.

1.2.2 Feynman's Path Integral Approach

When Richard Feynman was in graduate school, he noticed a remark in Paul Dirac's book that states that $\exp \left[i \int_{t_1}^{t_2} S \right]$ "corresponds to" $\langle x_2, t_2 | x_1, t_1 \rangle$ where

$$S = \int_{t_1}^{t_2} \frac{L(x, \dot{x})}{\hbar}, \quad L(x, \dot{x}) = T(\dot{x}) - V(x).$$

In this expression, T is the kinetic energy, V is the potential energy, L is the classical Lagrangian, and S is the classical action. By inserting completeness relations $\hat{\mathbb{1}} = \int |x, t\rangle \langle x, t| dx$ and splitting up the time interval $t_2 - t_1$ into infinitesimal intervals, it can be shown that the probability amplitude of a particle located at initial position x_i at time t_i being found at some other final location x_f at time t_f is

$$\langle x_f, t_f | x_i, t_i \rangle = \lim_{N \rightarrow \infty} \left(\frac{m}{2\pi i} \frac{N}{t_f - t_i} \right)^{N/2} \int dx_1 dx_2 \cdots dx_{N-1} e^{iS}. \quad (1.3)$$

This expression is for 1 dimension, but it can easily be generalized to 3 dimensions to obtain

$$\langle \mathbf{x}_f, t_f | \mathbf{x}_i, t_i \rangle = \lim_{N \rightarrow \infty} \left(\frac{m}{2\pi i} \frac{N}{t_f - t_i} \right)^{3N/2} \int d^3x_1 d^3x_2 \cdots d^3x_{N-1} e^{iS}. \quad (1.4)$$

This expression becomes exact when N goes to infinity, so it may seem like these integrals are impossible to evaluate. However, this result generalizes very nicely to lattice formalism where spacetime is discrete and finite. Thus, path integrals of the form of Eq. 1.4 can be evaluated on a lattice where each integral over d^3x_i corresponds to a time slice t_i of the Euclidean lattice. Since there is now a finite number of integrals, lattice formulation of Eq. 1.4 will have discretization errors but becomes more accurate as the lattice resolution

becomes sharper.

1.2.3 Euclidean Time

Lattice theory is often formulated using an imaginary time $t = -i\tau$, $\tau > 0$. This is called *Wick rotation*. This means that we use a Euclidean metric $g_{\mu\nu} = \delta_{\mu\nu}$ where $\delta_{\mu\nu}$ is the Kronecker delta, and intervals with 4-vectors $x_\mu = (-ix_0, \mathbf{x})$ (upper or lower indices no longer matter with a Euclidean metric) are now represented as $x_\mu g_{\mu\nu} x_\nu$. When t is replaced with $-i\tau$ and time derivatives are understood to be derivatives with respect to τ , the action S becomes

$$S = S_E = i \int (T + V) dt = i \int H_E dt = iS_E, \quad S_E \equiv \int H_E dt \quad (1.5)$$

where $H_E = \frac{1}{2m} \left| \frac{d\mathbf{x}}{d\tau} \right|^2 + V(\mathbf{x})$ is the Euclidean Hamiltonian. Now the path integral becomes

$$\langle \mathbf{x}_f, t_f | \mathbf{x}_i, t_i \rangle = \lim_{N \rightarrow \infty} \left(\frac{m}{2\pi i} \frac{N}{t_f - t_i} \right)^{3N/2} \int d^3x_1 d^3x_2 \cdots d^3x_{N-1} e^{-S_E}. \quad (1.6)$$

In classical mechanics, allowed trajectories $\mathbf{x}(t)$ satisfy $\delta S = 0$. That is, they minimize the action S . In quantum mechanics, all paths contribute to the path integral. However, e^{iS} in Eq. 1.4 rapidly oscillates for paths with large S such that paths far from the classically allowed trajectory do not contribute much to the integral. That is, the rapidly oscillating term causes a lot of cancellation. In the Euclidean path integral of Eq. 1.6, the oscillating e^{iS} is now an exponentially decaying e^{-S_E} , so that rapid oscillations are now replaced with exponential suppression for very non-classical paths in the integral.

1.2.3.1 Quantum Mechanics in Euclidean Time

Changing to Euclidean time affects other equations and objects in quantum mechanics in order to preserve various expressions involving 4-vectors. For instance, the gamma matrices in Minkowski spacetime γ^M satisfy

$$\{\gamma_\mu^M, \gamma_\nu^M\} = 2\eta_{\mu\nu} \quad (1.7)$$

where $\eta_{\mu\nu} = \text{diag}(1, -1, -1, -1)$ is the Minkowski metric. When we use Euclidean time, the metric should be replaced with the Euclidean metric so that

$$\{\gamma_\mu, \gamma_\nu\} = 2\delta_{\mu\nu}. \quad (1.8)$$

This is not possible to achieve, unless we modify the definition of the γ matrices. The anticommutation relation will hold if we define the Euclidean gamma matrices as

$$\gamma_4 = \gamma_0^M, \quad \gamma_i = -i\gamma_i^M, \quad i = 1, 2, 3 \quad (1.9)$$

where i denotes a spatial index. Note that while 0 is used as the temporal index in Minkowski spacetime, 4 is customarily used in Euclidean spacetime. Any γ_μ should be assumed to be defined with the Euclidean definition unless otherwise specified.

This definition of the gamma matrices modifies the appearance of the Dirac equation as well. Normally the Dirac equation reads

$$\left(p^\mu \gamma_\mu^M - m\right) \psi(x^\mu) = 0$$

where p^μ represents (p^0, \mathbf{p}) and γ_μ^M represents $(\gamma_0^M, \gamma_1^M, \gamma_2^M, \gamma_3^M)$. Summations over repeated indices (Einstein summation convention) are implied throughout. In Euclidean space-time, 4-vectors are denoted as

$$v^\mu = v_\mu = (v^1, v^2, v^3, v^4) = (v^1, v^2, v^3, iv^0)$$

where the distinction between upper (contravariant) and lower (covariant) indices does not matter, and the components of each 4-vector are equal to their contravariant Minkowski counterparts. Therefore, we can rewrite the operator in the Dirac equation as

$$p^\mu \gamma_\mu^M - m = -i \left(p^1 \gamma^1 + p^2 \gamma^2 + p^3 \gamma^3 \right) - ip^4 \gamma^4 - m = -ip_\mu \gamma_\mu - m.$$

Since the Euclidean metric makes no distinction between upper and lower indices, both indices in the implied summation can be written lower as they are in the above equation. However, Greek indices are still used to indicate that the sum is over 1,2,3,4 rather than just the spatial indices. However, Euclidean time treats time symmetrically with respect to space. As a consequence, the Dirac equation now reads

$$(-ip_\mu \gamma_\mu - m) \psi(x_\mu) = 0. \tag{1.10}$$

Similarly, the completeness relations for the Dirac spinors are also modified, now reading

$$\sum_{s=1,2} u^{(s)} \bar{u}^{(s)} = N (-ip_\mu \gamma_\mu + m), \quad \sum_{s=1,2} v^{(s)} \bar{v}^{(s)} = N (-ip_\mu \gamma_\mu - m), \tag{1.11}$$

where N is a normalization constant that depends on the normalization used for the bispinors.

$u^{(s)}$ are the regular solutions to the Dirac equation $(-ip_\mu\gamma_\mu - m)u^{(s)}(x_\mu) = 0$, $v^{(s)}$ are the negative energy solutions to $(-ip_\mu\gamma_\mu + m)v^{(s)}(x_\mu) = 0$, and the adjoint bispinor $\bar{u}^{(s)}$ is $\bar{u}^{(s)} = u^{(s)\dagger}\gamma_4$.

1.3 Quantum Field Theory

Quantum field theory (QFT) is the theory that comprehensively describes relativistic quantum mechanics and the fundamental interactions minus gravity. In classical and quantum mechanics, the primary degrees of freedom are the coordinates x, y, z . In a field theory, the degrees of freedom are the value of the field at each point in spacetime. Since spacetime is continuous, this results in infinite degrees of freedom. The Lagrangian formalism of classical mechanics can be carried over to QFT with the goal of finding a Lagrangian density \mathcal{L} such that the Euler-Lagrange equations yield the differential equation that the field satisfies, e.g. the Klein-Gordon equation, the Dirac equation. The Lagrangian density $\mathcal{L}(\phi, \partial_\mu\phi)$ describing a field $\phi(x_\mu)$ should be constructed such that

$$\frac{\partial\mathcal{L}}{\partial\phi} - \partial_\mu\frac{\partial\mathcal{L}}{\partial(\partial_\mu\phi)} = 0. \tag{1.12}$$

The path integral can be generalized to field theory by integrating over every value of space in addition to every value of time:

$$\begin{aligned}\langle \phi'(x_\mu) | \phi(y_\mu) \rangle &= \int \mathcal{D}[\phi] e^{iS}, \\ \int \mathcal{D}[\phi] &\equiv \lim_{N \rightarrow \infty} \int \mathcal{D}\phi_1 \cdots \mathcal{D}\phi_{N-1}, \\ \int \mathcal{D}\phi &\equiv \int \prod_{\mathbf{x}} d\phi(\mathbf{x}, t), \\ S &= \int \mathcal{L}(\phi, \partial_\mu \phi) d^4x.\end{aligned}\tag{1.13}$$

Chapter 2

Quantum Chromodynamics on the Lattice

2.1 Continuum QCD

2.1.1 The QCD Lagrangian, Gauge Fields, and Color Components

The theory of the strong interaction is quantum chromodynamics (QCD). It is mediated by gluon fields which are described by the potential $A_\mu(x)_{cd}$, which is a 4-vector (with Lorentz index μ) of 3×3 hermitian, traceless matrices (color indices c and d). They are elements of the Lie algebra $\text{su}(3)$. Together with the bispinor fields $\psi(x)_c^\alpha$ (here α is a Dirac index), the fermionic part of the QCD Lagrangian density can be written as

$$\mathcal{L}_F[\psi, \bar{\psi}, A] = \sum_{f=1}^{N_f} \bar{\psi}^{(f)}(x)_c^\alpha \left((\gamma_\mu)_{\alpha\beta} D_\mu(x)_{cd} + m^{(f)} \delta_{\alpha\beta} \delta_{cd} \right) \psi^{(f)}(x)_d^\beta \quad (2.1)$$

where

$$D_\mu(x)_{cd} = \delta_{cd} \partial_\mu + ig A_\mu(x)_{cd} \quad (2.2)$$

is the covariant derivative, g is the coupling strength between the fermionic and gauge fields, f is the flavor index, and N_f is the total number of flavors in consideration. The gauge field

part of the Lagrangian density is

$$\mathcal{L}_G[A] = \frac{1}{2} \text{tr} [F_{\mu\nu}(x)F_{\mu\nu}(x)]. \quad (2.3)$$

The field strength tensor $F_{\mu\nu}(x)$ is defined as

$$F_{\mu\nu}(x) \equiv -i[D_\mu(x), D_\nu(x)] = \partial_\mu A_\nu(x) - \partial_\nu A_\mu(x) + i[A_\mu(x), A_\nu(x)] \quad (2.4)$$

where the color indices have been suppressed. Since $A_\mu(x) \in \text{su}(3)$, we can decompose $A_\mu(x)$ into a superposition of the generators of SU(3) (which are the elements of the algebra $\text{su}(3)$):

$$A_\mu(x) = \sum_{i=1}^8 A_\mu^{(i)}(x)T_i, \quad T_i = \frac{1}{2}\lambda_i, \quad (2.5)$$

where λ_i are the Gell-Mann matrices. This first summation is explicitly written despite the repeated index to emphasize that this sum runs from 1 to 8 (over color components). The 4-vectors $A_\mu^{(i)}(x)$ are the *color components* of the gauge field. Thus, the field strength tensor can be written as

$$F_{\mu\nu}(x) = \sum_{i=1}^8 F_{\mu\nu}^{(i)}(x)T_i \quad (2.6)$$

$$F_{\mu\nu}^{(i)}(x) = \partial_\mu A_\nu^{(i)}(x) - \partial_\nu A_\mu^{(i)}(x) - f_{ijk}A_\mu^{(j)}(x)A_\nu^{(k)}(x),$$

where the structure constants f_{ijk} are defined by the relation $[T_i, T_j] = if_{ijk}T_k$. Thus, the gauge field part of the Lagrangian density can be written as

$$\mathcal{L}_G[A] = \frac{1}{4}F_{\mu\nu}^{(i)}(x)F_{\mu\nu}^{(i)}(x), \quad (2.7)$$

where the trace of products of T_i is evaluated with the relation $\text{tr}[T_i T_j] = \frac{1}{2} \delta_{ij}$. The full QCD action is thus

$$S[\psi, \bar{\psi}, A] = \int d^4x (\mathcal{L}_F[\psi, \bar{\psi}, A] + \mathcal{L}_G[A]). \quad (2.8)$$

2.1.2 Local Gauge Invariance

The Lagrangian density has its form so that it is invariant under local SU(3) gauge transformations. These transformations modify the fields as

$$\psi'(x) = \Omega(x)\psi(x), \quad \bar{\psi}'(x) = \bar{\psi}(x)\Omega(x)^\dagger, \quad A'_\mu(x) = \Omega(x)A_\mu(x)\Omega(x)^\dagger + i(\partial_\mu\Omega(x))\Omega(x)^\dagger, \quad (2.9)$$

for $\Omega(x) \in \text{SU}(3)$. $A_\mu(x)$ must transform like this so that the covariant derivative transforms as

$$D'_\mu(x) = \Omega(x)D_\mu(x)\Omega(x)^\dagger. \quad (2.10)$$

Because $F_{\mu\nu}(x)$ is the commutator of covariant derivatives, it transforms as

$$F'_{\mu\nu}(x) = \Omega(x)F_{\mu\nu}(x)\Omega(x)^\dagger. \quad (2.11)$$

This ensures that $S[\psi', \bar{\psi}', A'] = S[\psi, \bar{\psi}, A]$.

2.2 QCD Actions on the Lattice

The following subsection is largely based on [2], and the notation used there largely matches the notation used here.

2.2.1 Lattice Gauge Invariance and Link Variables

2.2.1.1 Fermionic Part

The Lagrangian density and action introduced in the previous section apply to the continuum, but the expressions in Eqs. 2.1, 2.3, and 2.8 are not suitable for the lattice in their current form. This is because of the derivative term which must be discretized on the lattice. Let $x = an$ where a is the lattice spacing and $n = (\mathbf{n}, n_4)$ is a vector of integers which denotes which lattice site is referenced, e.g. $n_i \in \{0, 1, \dots, N - 1\}$, $n_4 \in \{0, 1, \dots, N_T - 1\}$ on an $N^3 \times N_T$ lattice. From hereon, $\psi(n)$ is understood to mean the value of the field ψ at position an . Thus, the gradient on the lattice is given by

$$\partial_\mu \psi(x) = \frac{\psi(n + \hat{\mu}) - \psi(n - \hat{\mu})}{2a} + \mathcal{O}(a), \quad (2.12)$$

where $\hat{\mu}$ is a vector of length a in the μ -direction. Then the discretized version of the fermionic part of the action for a free fermion becomes

$$S_F [\psi, \bar{\psi}] = \int \mathcal{L}_F [\psi, \bar{\psi}] d^4x \rightarrow a^4 \sum_{n \in \Lambda} \bar{\psi}(n) \left(\gamma_\mu \frac{\psi(n + \hat{\mu}) - \psi(n - \hat{\mu})}{2a} + m\psi(n) \right),$$

where Λ is the set of all spacetime points on the lattice, and the integral is replaced with a discrete sum. This presents a problem for gauge invariance because when ψ is replaced with ψ' , then we are left with terms like

$$\bar{\psi}'(n)\psi'(n \pm \hat{\mu}) = \bar{\psi}(n)\Omega(n)^\dagger \Omega(n \pm \hat{\mu})\psi(n \pm \hat{\mu}) \neq \bar{\psi}(n)\psi(n \pm \hat{\mu}).$$

The solution is to introduce a new field $U_\mu(n)$ that transforms under a gauge transformation as

$$U'_\mu(n) = \Omega(n)U_\mu(n)\Omega(n + \hat{\mu})^\dagger. \quad (2.13)$$

These are called *link variables* because they link site n with the site that is one site away from n in the $\hat{\mu}$ -direction through this gauge transformation property. A negative direction may also be specified, and $U_\mu(n)$ is defined such that

$$U_{-\mu}(n) \equiv U_\mu(n - \hat{\mu})^\dagger, \quad (2.14)$$

as shown in Fig. 2.1.

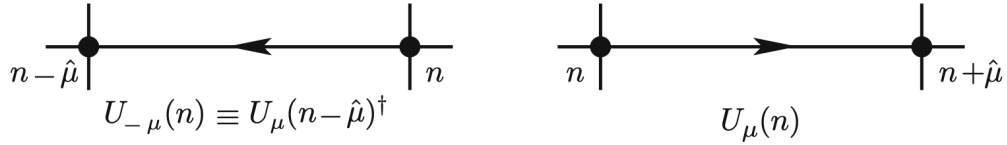


Figure 2.1: The link variable $U_\mu(n)$ (right) links lattice site n with site $n + \hat{\mu}$ and is directed in the $\hat{\mu}$ -direction. The link variable $U_{-\mu}(n)$ (left) links n with $n - \hat{\mu}$ and is directed in the $-\hat{\mu}$ -direction. The definition the hermitian conjugate of the link variables is also displayed. Image source [2].

Now we note that

$$\bar{\psi}'(n)U'_{\pm\mu}(n)\psi'(n \pm \hat{\mu}) = \bar{\psi}(n)U_{\pm\mu}(n)\psi(n \pm \hat{\mu})$$

is a gauge-invariant construct and try as a candidate for the fermionic action

$$S_F[\psi, \bar{\psi}, U] = a^4 \sum_{n \in \Lambda} \bar{\psi}(n) \left(\gamma_\mu \frac{U_\mu(n)\psi(n + \hat{\mu}) - U_{-\mu}(n)\psi(n - \hat{\mu})}{2a} + m\psi(n) \right). \quad (2.15)$$

Although this is gauge invariant, we must still determine what U could be. It turns out that

the path-ordered exponential

$$P \exp \left(i \int_{\mathcal{C}} A_{\mu} ds_{\mu} \right),$$

along some contour \mathcal{C} , has the gauge transformation property required by Eq. 2.13. Here the coupling g has been absorbed into the field A_{μ} . Since U_{μ} connects adjacent lattice sites that are a small distance apart, the integral can be approximated such that

$$U_{\mu}(n) = \exp (iaA_{\mu}(n)). \quad (2.16)$$

To see that Eq. 2.15 with U instead of A is correct, we see that when Eq. 2.16 is expanded through order $\mathcal{O}(a)$, the action becomes

$$S_F [\psi, \bar{\psi}, A] = a^4 \sum_{n \in \Lambda} \bar{\psi}(n) \left[\gamma_{\mu} \left(\frac{\psi(n + \hat{\mu}) - \psi(n - \hat{\mu})}{2a} + iaA_{\mu}(n) + \mathcal{O}(a) \right) + m\psi(n) \right], \quad (2.17)$$

which matches Eq. 2.1 if one attempts to naively discretize this expression to use on the lattice. Thus, it is clear that the correct gauge degrees of freedom on the lattice are $U_{\mu}(n)$ instead of $A_{\mu}(n)$.

2.2.1.2 Gauge Part

Since the correct gauge field to use on the lattice is U , the expression for the gauge part of the action $S_G[A]$ must also be modified. The trace of a product of link variables that trace a closed contour is gauge-invariant, so this is the type of object that will be used to construct the action. The simplest contour of this type is the *plaquette* as illustrated in Fig. 2.2. It is a closed contour made of 4 link variables that make a planar square.

The plaquette specifies two directions μ and ν for the directions of the links. If we wish

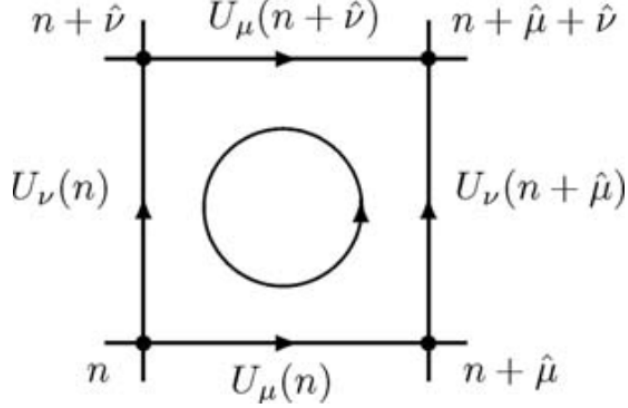


Figure 2.2: A counter-clockwise plaquette in the $\hat{\mu}$ - and $\hat{\nu}$ -directions. The links that appear to go against the orientation of the loop ($U_\mu(n + \hat{\nu})$ at the top and $U_\nu(n)$ to the left) are actually written to go in the positive $\hat{\mu}$ - and $\hat{\nu}$ -directions because the diagram is meant to show the relevant link variables written in standard form such that they point in the positive directions. Thus, the link variables that appear in the plaquette are $U_\mu(n + \hat{\nu})^\dagger$ and $U_\nu(n)^\dagger$. Image from [2].

to traverse in the μ -direction first, then we write the plaquette as

$$U_{\mu\nu}(n) = U_\mu(n)U_\nu(n + \hat{\mu})U_{-\mu}(n + \hat{\mu} + \hat{\nu})U_{-\nu}(n + \hat{\nu}) = U_\mu(n)U_\nu(n + \hat{\mu})U_\mu(n + \hat{\nu})^\dagger U_\nu(n)^\dagger. \quad (2.18)$$

The *Wilson gauge action* is constructed by summing over all plaquettes in a single orientation on the lattice:

$$S_G[U] = \frac{2}{g^2} \sum_{n \in \Lambda} \sum_{\mu < \nu} \text{Re tr} [1 - U_{\mu\nu}(n)]. \quad (2.19)$$

The second summation requires $\mu < \nu$ because when μ and ν are swapped, the plaquette reverses orientation, and if $\mu = \nu$, then the plaquette has nonsensical meaning (actually it does not contribute to the summation because $U_{\mu\mu} = 1$). If $U_{\mu\nu}(n)$ is rewritten with the Baker-Campbell-Hausdorff formula up to the first term with a commutator, then if $U_{\mu\nu}(n)$

is expanded to lowest non-vanishing order in Eq. 2.19, we find that

$$S_G[U] = \frac{2}{g^2} \sum_{n \in \Lambda} \sum_{\mu < \nu} \text{Re tr} [1 - U_{\mu\nu}(n)] = \frac{a^4}{2g^2} \sum_{n \in \Lambda} \sum_{\mu, \nu} \left(\text{tr} [F_{\mu\nu}(n)^2] + \mathcal{O}(a^2) \right).$$

This matches Eq. 2.3 to lowest order, except once again, A has been rescaled to absorb a factor of g such that $1/g^2$ appears in the expression. The sum over $\mu < \nu$ has been replaced with an unconstrained sum over μ and ν with a factor of $1/2$ to account for the fact that this double-counts terms (also the sum over μ, ν is explicitly written out instead of implied like in Eq. 2.3).

2.3 Evaluating Lattice Quantities

2.3.1 Calculating Lattice Quantities

Now we can write the entire action as

$$S[\psi, \bar{\psi}, U] = S_F[\psi, \bar{\psi}, U] + S_G[U],$$

and we can use this to evaluate the path integral on the lattice. In Eq. 1.6, there are similarities to the types of integrals that one performs in statistical physics calculations where the Boltzmann factor is e^{-SE} . In addition, the amplitude $\langle \mathbf{x}_f, T | \mathbf{x}_i, 0 \rangle$ can be written as $\langle \mathbf{x}_f | e^{-T\hat{H}} | \mathbf{x}_i \rangle$ where $e^{-T\hat{H}}$ looks like the canonical density operator $\hat{\rho} = e^{-\beta\hat{H}}$ where $\beta \rightarrow T$. That is, the size of the time evolution acts as an inverse temperature in the Euclidean

LQCD theory. This suggests defining the partition function as

$$Z_T = \text{tr} \left[e^{-T\hat{H}} \right] = \int \mathcal{D}\psi_0 \mathcal{D}\bar{\psi}_0 \mathcal{D}U_0 \langle \psi_0, \bar{\psi}_0, U_0 | e^{-T\hat{H}} | \psi_0, \bar{\psi}_0, U_0 \rangle. \quad (2.20)$$

However, the matrix element in the integrand can be evaluated with the path integral formalism if we generalize Eq. 1.6 to fields. Then the partition function on the lattice becomes

$$\begin{aligned} Z_T &= \int \mathcal{D}[\psi, \bar{\psi}] \mathcal{D}[U] e^{-S[\psi, \bar{\psi}, U]}, \\ \mathcal{D}[\psi, \bar{\psi}] &= \prod_{n \in \Lambda} \prod_{f, \alpha, c} d\psi^{(f)}(n)_\alpha d\bar{\psi}^{(f)}(n)_\alpha, \\ \mathcal{D}[U] &= \prod_{n \in \Lambda} \prod_{\mu=1}^4 dU_\mu(x). \end{aligned} \quad (2.21)$$

Overall multiplicative factors that appear outside of the integral in equations like Eq. 1.6 are omitted because they cancel out in relevant calculations. This motivates defining expectation values as

$$\langle O_2(t) O_1(0) \rangle \equiv \frac{1}{Z_T} \text{tr} \left[\hat{O}_2(t) \hat{O}_1(0) \hat{\rho} \right] = \frac{1}{Z_T} \text{tr} \left[e^{-\hat{H}(T-t)} \hat{O}_2 e^{-\hat{H}t} \hat{O}_1 \right], \quad (2.22)$$

where in the second equality, the cyclic invariance of traces and Heisenberg time-evolution of operators are used. This particular example is a 2pt correlation function, but it can be generalized to simpler or more complex observables as well. It will be assumed that the operators \hat{O} are functions of the relevant fields (and not any conjugate fields, e.g. conjugate momentum), i.e. $\hat{O} = \hat{O}[\hat{\psi}, \hat{\bar{\psi}}, \hat{U}]$. The same methodology used to derive Eqs. 1.4, 1.6, and

2.21 shows that Eq. 2.22 can also be evaluated in the path integral approach and becomes

$$\begin{aligned} \langle O_2(t)O_1(0) \rangle &= \frac{1}{Z_T} \int \{ \mathcal{D} [\psi, \bar{\psi}] \mathcal{D}[U] O_2 [\psi(\mathbf{n}, n_t), \bar{\psi}(\mathbf{n}, n_t), U(\mathbf{n}, n_t)] \\ &\quad \times O_1 [\psi(\mathbf{n}, 0), \bar{\psi}(\mathbf{n}, 0), U(\mathbf{n}, 0)] e^{-S[\psi, \bar{\psi}, U]} \} \end{aligned} \quad (2.23)$$

Because these integrals are identical in form to the integrals used to evaluate quantities in statistical physics, the same numerical techniques can be used here to calculate lattice quantities as well. However, the calculation of lattice quantities from actual lattice configurations is outside the scope of this thesis.

2.3.2 Spectral Decomposition of Lattice Quantities

Once an observable has been calculated from Eq. 2.23, it is analyzed through a spectral decomposition of the observable and the partition function. Now it is better to evaluate the trace using a complete basis of energy eigenstates in addition to the identity operator as the sum over projections to energy eigenstates $\mathbb{I} = \sum_n |n\rangle\langle n|$.¹ Thus, the partition function becomes

$$Z_T = \sum_n e^{-E_n T} \approx 1 \text{ for sufficiently large } T, \quad (2.24)$$

where $E_{n+1} > E_n$. Then Eq. 2.23 becomes

$$\langle O_2(t)O_1(0) \rangle \approx \sum_{m,n} \langle m|O_2|n\rangle \langle n|O_1|m\rangle e^{-E_m(T-t)} e^{-E_n t} \approx \sum_n \langle 0|O_2|n\rangle \langle n|O_1|0\rangle e^{-E_n t}, \quad (2.25)$$

where in the last approximation it is once again assumed that T is sufficiently large.

¹This definition can be modified depending on normalization conventions, e.g. $\mathbb{I} = \sum_n \frac{|n\rangle\langle n|}{2E_n}$ for Klein-Gordon fields with Lorentz-invariant normalization, i.e. $\langle \mathbf{p}|\mathbf{p}' \rangle = 2E(|\mathbf{p}|)(2\pi)^3 \delta^3(\mathbf{p} - \mathbf{p}')$.

Now that the groundwork for lattice theory has been laid down, the rest of this thesis is organized as follows. Chapter 3 explains how lattice correlator data is analyzed in order to extract physical observables. I begin with the definitions of the 2pt and 3pt lattice correlators. Then I explain how the correlator data is fitted and how useful quantities are extracted from the fit (Sec. 3.1). Next, in Chapter 4, I explain how to calculate the renormalization constants to perform non-perturbative renormalization (NPR) of the gluon energy-momentum tensor (EMT). I explain what quantities are needed for the calculation and how to calculate different parts of the renormalization constant using the RI/MOM scheme (Secs. 4.1-4.3), including the CDER technique to improve the signal (Sec. 4.2). I also explain the workflow for the different steps required to turn the lattices into results (Sec. 4.4). Next I explain how those quantities are used to calculate the EM form factors, after which I show how the form factors are used to calculate the electric radius, magnetic radius, and magnetic moment (PENDING). Then, I extrapolate the lattice results to the continuum limit to obtain values that can be compared to experiment and other theory (PENDING). Finally, I present a conclusion and summary of my work in Chapter 6.

Chapter 3

Analyzing Lattice Correlator Data

3.1 The 2pt and 3pt Correlators

The particular lattice quantities required for the analysis of the electromagnetic form factors are the 2pt and 3pt correlation functions (the correlation functions are also referred to as simply correlators). For this particular project, I analyzed spin-1/2 particles that obey the Dirac equation, and the identity operator required by the normalization used in my data is

$\mathbb{I} = \sum_{n_s} \frac{M_N}{E_N} |n_s\rangle\langle n_s|$ where the sum is over spins s as well as energy eigenstates n . The 2pt correlators are defined very similarly to Eq. 2.23 as

$$C^{2\text{pt}}(\mathbf{p}, t) = \langle \chi_B(\mathbf{p}, t) \bar{\chi}_B(\mathbf{p}, 0) \rangle = \sum_n Z_n(|\mathbf{p}|) \langle 0 | \chi_B(\mathbf{p}) | n \rangle \langle n | \bar{\chi}_B(\mathbf{p}) | 0 \rangle e^{-E_n t}, \quad (3.1)$$

where $\bar{\chi}_B(\mathbf{p}, 0)$ is an operator that creates baryon B with momentum \mathbf{p} at time 0 and $\chi_B(\mathbf{p}, t)$ annihilates it at time t . Usually the baryon is instead created at some position and is annihilated after undergoing some displacement \mathbf{x} , then Fourier transformed to the momentum of interest.

The 3pt correlators are defined as

$$\begin{aligned}
C^{\text{3pt}}(\mathbf{p}_f, \mathbf{p}_i, \tau, t) &= \langle \chi_B(\mathbf{p}_f) V(\mathbf{q}) \bar{\chi}_B(\mathbf{p}_i) \rangle \\
&= \sum_{m,n} Z_m(|\mathbf{p}_i|) Z_n(|\mathbf{p}_f|) \langle 0 | \chi_B(\mathbf{p}_f) | n \rangle \langle n | V(\mathbf{q}) | m \rangle \langle m | \bar{\chi}_B(\mathbf{p}_i) | 0 \rangle \quad (3.2) \\
&\quad \times e^{-E_n(\tau-t)} e^{-E_m t}.
\end{aligned}$$

This corresponds to a particle created at time 0 with 3-momentum \mathbf{p}_i at time 0 that interacts with operator $V(\mathbf{q} = \mathbf{p}_f - \mathbf{p}_i)$ at time t that imparts momentum transfer \mathbf{q} that is then annihilated at time τ with 3-momentum \mathbf{p}_f . The V operator corresponds to some property of the particle that we want to study. As a result, the 3pt correlator is only defined for $0 \leq t \leq \tau$ since the particular cannot be inspected after it is annihilated. The Z terms in Eqs. 3.1 and 3.2 are kinematic factors that depend on the normalization, e.g. $Z_n(|\mathbf{p}|) = M/E_n(|\mathbf{p}|)$ for spin-1/2 particles. For spin-1/2 particles, the creation and annihilation operators have Dirac indices, so the expressions in Eqs. 3.1 and 3.2 must be contracted by a projection operator to select out the relevant spin projections. “Relevant” depends on the quantity that we are trying to calculate by using the correlators.

In order to calculate the gluon momentum fraction of the nucleon, the V operator is the gluon energy-momentum tensor, and this operator is placed between two nucleon ground states as $\langle 0 | V | 0 \rangle$. This can be extracted from the 3pt correlator by fitting sampled 3pt correlator data and using fitted sampled 2pt correlator data to divide out the unwanted terms and kinematic factors in Eq. 3.2.

3.1.1 Fitting the 2pt Correlator

It should be noted that the following sections involve analyzing data that comes from lattice simulations of QCD, i.e. the 2pt and 3pt correlators. For my analysis, these were provided to me to analyze, as I was not involved in taking the data. In addition, any time values that appear in the following sections should be interpreted to be integer values, i.e. they correspond to lattice grid indices. This means that the exponential terms in equations like Eqs. 3.1 and 3.2 contain the unitless energy aE_n and the unitless integer time t as the lattice spacing a is attached to the energy rather than the time. However, the energy will still be written as E_n even though it is implied to be the unitless aE_n .

The first step to analyzing correlator data is performing 2pt correlator fits. Given N_{cfg} samples of the 2pt correlator as a function of time from lattice calculations, the first step taken is jackknife resampling of the N_{cfg} configurations. Jackknife resampling is important because the nonlinearity of the quantities calculated with the correlators. By using the raw data without resampling, the mean of such quantities has a bias that goes as $O(1)$, i.e. increasing the number of samples does not improve the convergence to the true mean. With jackknife resampling, these calculated quantities have a bias that goes as $O(1/N_{\text{cfg}})$, so with jackknife resampling, we will converge to the true mean with more data [3].

For the purposes of curve fitting, Eq. 3.1 is written as

$$C^{2\text{pt}}(t) = \sum_n |A_n|^2 e^{-E_n t} = |A_0|^2 e^{-E_0 t} + |A_1|^2 e^{-E_1 t} + \dots \quad (3.3)$$

such that the specific matrix elements are ignored for fitting purposes and normalization or kinematic factors are absorbed into the A_n . The fit parameters are then $|A_n|^2$ and E_n . Although it is not written for brevity, the 2pt correlator corresponds to one momentum,

and thus the fit parameters are momentum-dependent. This means that each correlator corresponds to a different $|\mathbf{p}|$, where the only dependence is on the magnitude due to the isotropy of space (which means that the choice to only have nonzero p_z is arbitrary). The number of states/terms included in the fit depends on how many can be resolved in the data.

I present an example of 2pt correlator (and subsequently 3pt correlator analysis) using the data from the lattice ensembles that are used for non-perturbative renormalization (NPR) in Chapter 4, where the ensembles are explained in more detail (see Table 4.1). I used a 2-state fit for this data. However, not all of the data is used for fitting. The lowest values of t have too much excited state contamination to be used, and the highest values of t end up having too much noise compared to signal. Therefore, a proper subset of the range $[0, L_t]$ is used, and selecting it is non-trivial. In order to determine a good t range to use, I start by making a so-called *effective mass*¹ plot. The effective mass is given by $\ln [C^{2\text{pt}}(t)/C^{2\text{pt}}(t+1)]$. As t increases, Eq. 3.3 becomes dominated by just the ground state term, the effective mass asymptotically approaches E_0 , and the plot should approach a horizontal line for this range of $t \gg 0$. This is visible in Fig. 3.1 where the effective mass is plotted with the reconstructed fit band obtained by using the fitted parameters in the fitted equation.

The reconstructed fit bands in Fig. 3.1 are created by fitting the 2pt correlator to Eq. 3.3 and then calculating the effective mass with $\ln [C^{2\text{pt}}(t)/C^{2\text{pt}}(t+dt)]/dt$ with the fitted parameters. Note that dt replaces 1 (and there is division by dt) because the fitted band uses many interpolated values at t that have smaller spacing than that of the data points.

For this particular data, a 2-state fit was performed, which means that the data was fitted

¹*Effective mass* is a bit of a misnomer because it only corresponds to the mass if the 2pt correlator is projected to zero momentum; otherwise it corresponds to the ground state energy, which will have a kinetic contribution. However, I've never heard anyone call it a *ground state energy* plot.

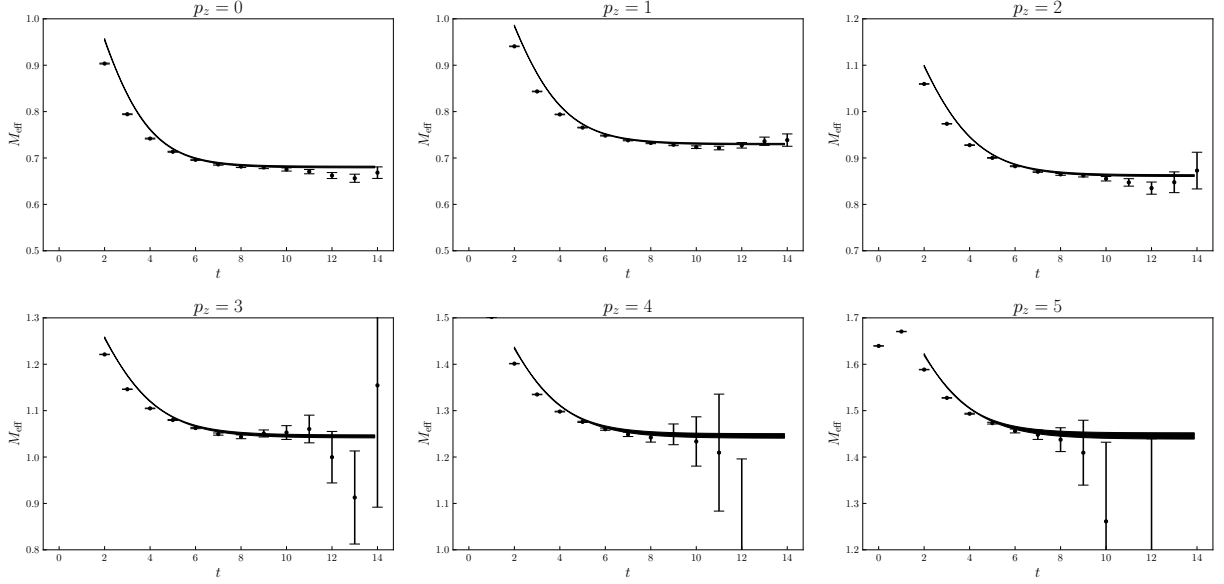


Figure 3.1: Effective mass plots and reconstructed fit bands for the a12m310 ensemble for $p_z = [0, 5]$ in units of $2\pi/(aL)$. Fits were performed with $t \in [2, 11]$. The fit bands were extended to all available t (they exceed $t = 11$) to demonstrate that the effective mass approaches E_0 . The y -axis range was chosen so that the most important features of the data can be better visualized, but this caused some of the data points for the highest t to not be visible for $p_z = 4, 5$.

to

$$C^{2\text{pt}}(t) = |A_0|^2 e^{-E_0 t} + |A_1|^2 e^{-E_1 t}. \quad (3.4)$$

In order to determine a suitable fit range, I examined the effective mass plots (without the fit bands because they are calculated from the fit which had yet to be performed) and picked t bounds such the fit range includes some of the data points before they approach a horizontal line and most of the data after this occurs. However, not all of the available data after the lower bound is used because eventually the data starts to become noisier and also deviates from the asymptotic value of the other nearby data points. For example, for $p_z = 0$, the effective mass at $t = [12, 14]$ is noticeably lower than the asymptotic value approached at $t = [6, 11]$. Even though these phenomena appear at different t for different p_z , this fit range was used for all p_z for consistency. All of the fits have $\chi^2/\text{dof} < 1$ except for $p_z = 1$ where

it is still close to 1. This suggests that the fits are good quality, and with the lowest χ^2/dof being around 0.3, the data does not appear to be overfitted. For smaller t , the fitted band decreases with t due to the presence of excited states. Eventually, the fit band approaches a horizontal line as the 2pt correlator becomes dominated by only the ground state term. The results of the fits are summarized in Table 3.1.

p_z	$ A_0 ^2$	E_0	$ A_1 ^2$	E_1	χ^2/dof
0	7.705(97)e-10	0.681(2)	2.088(30)e-9	1.455(14)	0.808(254)
1	2.684(28)e-9	0.730(1)	6.491(59)e-9	1.448(10)	1.234(322)
2	8.469(120)e-9	0.862(2)	1.839(15)e-8	1.531(12)	1.100(360)
3	2.444(57)e-8	1.044(3)	4.542(41)e-8	1.696(20)	0.692(248)
4	6.057(205)e-8	1.245(5)	9.529(95)e-8	1.894(32)	0.397(356)
5	1.225(56)e-7	1.445(7)	1.728(16)e-7	2.092(44)	0.397(587)

Table 3.1: Fit parameters from fitting the 2pt correlator to Eq. 3.4 and the corresponding χ^2/dof for the a12m310 ensemble for $p_z \in [0, 5] \times 2\pi/(aL)$. Fits were performed using $t \in [2, 11]$. The energy parameters are actually the unitless aE_n , i.e. they are in lattice units.

3.1.2 Fitting the 3pt Correlator

After fitting the 2pt correlator, I fitted the 3pt correlator as well. Just as how Eq. 3.1 was rewritten as Eq. 3.3, in practice, we rewrite Eq.3.2 as

$$C^{3\text{pt}}(\mathbf{p}_f, \mathbf{p}_i, \tau, t) = \sum_{m,n} |A_m(\mathbf{p}_f)| |A_n(\mathbf{p}_i)| \langle m|V|n\rangle e^{-E_m(\tau-t)} e^{-E_n t}, \quad (3.5)$$

where normalization or kinematic factors are once again absorbed into the A_m and A_n . It is important to fit the 2pt correlator first because in practice, we do not fit the energy parameters in Eq. 3.2 but rather insert the values obtained from the 2pt correlator fits. This makes finding the optimal parameters much easier as the time-dependence in the 3pt correlator is more complex than that of the 2pt correlator. Thus, it is preferable to avoid having fit

parameters that are directly multiplied by time. For this particular work, the operator V was the gluon energy-momentum tensor (EMT) which I will label as O_g , consistent with our work in Ref. [4], given by

$$O_{g,\mu\nu} = F_{\mu\rho}F_{\nu\rho} - \frac{1}{4}g_{\mu\nu}F_{\rho\sigma}F_{\rho\sigma}. \quad (3.6)$$

In particular, we used $O_{g,44}$ (the time-diagonal component, called $O_{g,tt}$ in [4]), for which $\langle 0|O_{g,44}|0\rangle$ is proportional to $\langle x\rangle_g E_0$, where $|0\rangle$ is the nucleon ground state, E_0 is the nucleon ground state energy, and $\langle x\rangle_g$ is the fraction of momentum carried by the gluons. The EMT was projected to zero momentum transfer so that $\mathbf{p}_i = \mathbf{p}_f$.

Just as with the 2pt correlator, I fitted to the first excited state diagonal term, i.e. up to $m = n = 1$. Thus, the fit function was

$$\begin{aligned} C^{3pt}(\tau, t) = & |A_0|^2 \langle 0|O_g|0\rangle e^{-E_0\tau} + |A_0||A_1| \langle 0|O_g|1\rangle e^{-E_0(\tau-t)} e^{-E_1t} \\ & + |A_1||A_0| \langle 0|O_g|1\rangle e^{-E_1(\tau-t)} e^{-E_0t} + |A_1|^2 \langle 1|O_g|1\rangle e^{-E_1\tau}, \end{aligned} \quad (3.7)$$

where momentum labels have been omitted for brevity. This equation simplifies from the form of Eq. 3.2 because of the identical initial and final momenta/lack of momentum transfer. Because the energies from the 2pt correlator fit are inserted into this equation, the only fitted parameters are the $\langle m|O_g|n\rangle$. Additionally, because the initial and final momenta are the same, the states $|m\rangle$ and $|n\rangle$ are at the same momentum, so when $m = n$, they describe identical states. Thus, $\langle 1|O_g|0\rangle = \langle 0|O_g|1\rangle^*$. Furthermore, because the matrix elements of the EMT are real, we have $\langle 1|O_g|0\rangle = \langle 0|O_g|1\rangle$. This means that there are only 3 parameters to fit rather than 4 (8 if the real and imaginary parts of complex parameters are considered separate) despite the presence of 4 matrix elements in Eq. 3.7. After fitting, the

$|A_m||A_n$ are divided out if necessary so that we are left with only the matrix element (and kinematic factors that must also be removed).

In order to choose the fit range, we observe that for $t \gg 0$ and $t \ll \tau$, Eq. 3.5 is dominated by the ground state term ($m = n = 0$). This corresponds to the middle-most t between 0 (creation) and τ (annihilation). If suitable t and τ are used such that both the 3pt and 2pt correlators are dominated by the ground state, then the special ratio

$$\mathcal{R} = \frac{C^{3\text{pt}}(\mathbf{p}_f, \mathbf{p}_i, \tau, t)}{C^{2\text{pt}}(\mathbf{p}_i, \tau)} \sqrt{\frac{C^{2\text{pt}}(\mathbf{p}_i, t)C^{2\text{pt}}(\mathbf{p}_i, \tau)C^{2\text{pt}}(\mathbf{p}_f, \tau - t)}{C^{2\text{pt}}(\mathbf{p}_f, t)C^{2\text{pt}}(\mathbf{p}_f, \tau)C^{2\text{pt}}(\mathbf{p}_i, \tau - t)}} \quad (3.8)$$

approaches the ground state matrix element for $0 \ll t \ll \tau$. Since we have $\mathbf{p}_i = \mathbf{p}_f = \mathbf{p}$, the square root term is 1 and Eq. 3.8 becomes a simple ratio of $C^{3\text{pt}}(\mathbf{p}, \tau, t)/C^{2\text{pt}}(\mathbf{p}, \tau)$. In this limit of t , a plot of Eq. 3.8 approaches a plateau at that matrix element (for $\mathbf{p}_i \neq \mathbf{p}_f$, it can look more like a stationary inflection rather than a local maximum). To determine a suitable fit range, we plot this ratio as a function of t for multiple choices of τ and examine the plateaus. Because agreement with this limit is strongest when t is exactly in the middle of 0 and τ , we symmetrically exclude endpoints such that t_{cut} points are excluded from each side, so the fit range becomes $t \in [t_{\text{cut}}, \tau - t_{\text{cut}}]$ for each τ . Much like the effective mass plot analysis, when excited states are desired in the fit, we make sure to include some t outside of the plateau region since the plateau arises when only the ground state is dominant. When 3pt correlator data with multiple τ are fitted as part of a single fit, this is called a *simultaneous fit* or “sim fit,” and the fit function is essentially a function of multiple variables (t and τ). Since we included terms in the fit function up to the first excited (two states altogether), we refer to these 3pt correlator fits as “two-sim fits.” Using the same lattice configurations that were used for the 2pt correlator analysis in the previous section, I fitted the 3pt correlator

for the a12m310 ensemble using $\tau \in [7, 11]$ and $t_{\text{cut}} = 1$. The fitted parameters and fit functions for both the 3pt and 2pt correlators are then used to make reconstructed fit bands of Eq. 3.8, and these bands are plotted with the original data points and a horizontal band to denote the location of the ground state matrix element $\langle 0|O_{g,tt}|0\rangle$ in Fig. 3.2.

Only the real part of the correlators and ratio produce a signal for the gluon EMT. Because different values of τ result in different ranges of t such that the largest t is τ , the data is plotted vs. $t - \tau/2$ (rather than t) so that the data for each τ is centered around the middle of the plot at $t - \tau/2 = 0$. Otherwise, if all τ were plotted on the same plot, they would not align very well as the data for different τ would end at different t . With this choice of the horizontal axis, the data for different τ should overlap at $t - \tau/2 = 0$ and approach the value of $\langle 0|O_{g,tt}|0\rangle$, so it is easier to determine qualitatively if the data behave as expected. In order to convert $\langle 0|O_{g,tt}|0\rangle$ into $\langle x \rangle_g^{\text{bare}}$, a kinematic factor must be divided out.

In Fig. 3.2, the gray band denoting $\langle 0|O_{g,tt}|0\rangle$ and plateau region (near $t - \tau/2 = 0$) of the reconstructed fit bands intersect as expected. For $p_z \geq 3 \times 2\pi/(aL)$, the error on the data points become noticeably larger such that the data for the largest τ no longer form a clear plateau. The same occurs for increasing τ , although the increase in the amount of error is greater as p_z increases. This causes the data for the largest p_z and τ to no longer form a clear plateau. As a result, the vertical axis range for $p_z = 4, 5 \times 2\pi/(aL)$ is reduced so that the gray band and data with smaller error can be seen more clearly. This results in error bars for the largest τ extending past the vertical range. All of the fits have $\chi^2/\text{dof} < 1$. The fitted parameters and matrix element are displayed in Table 3.2.

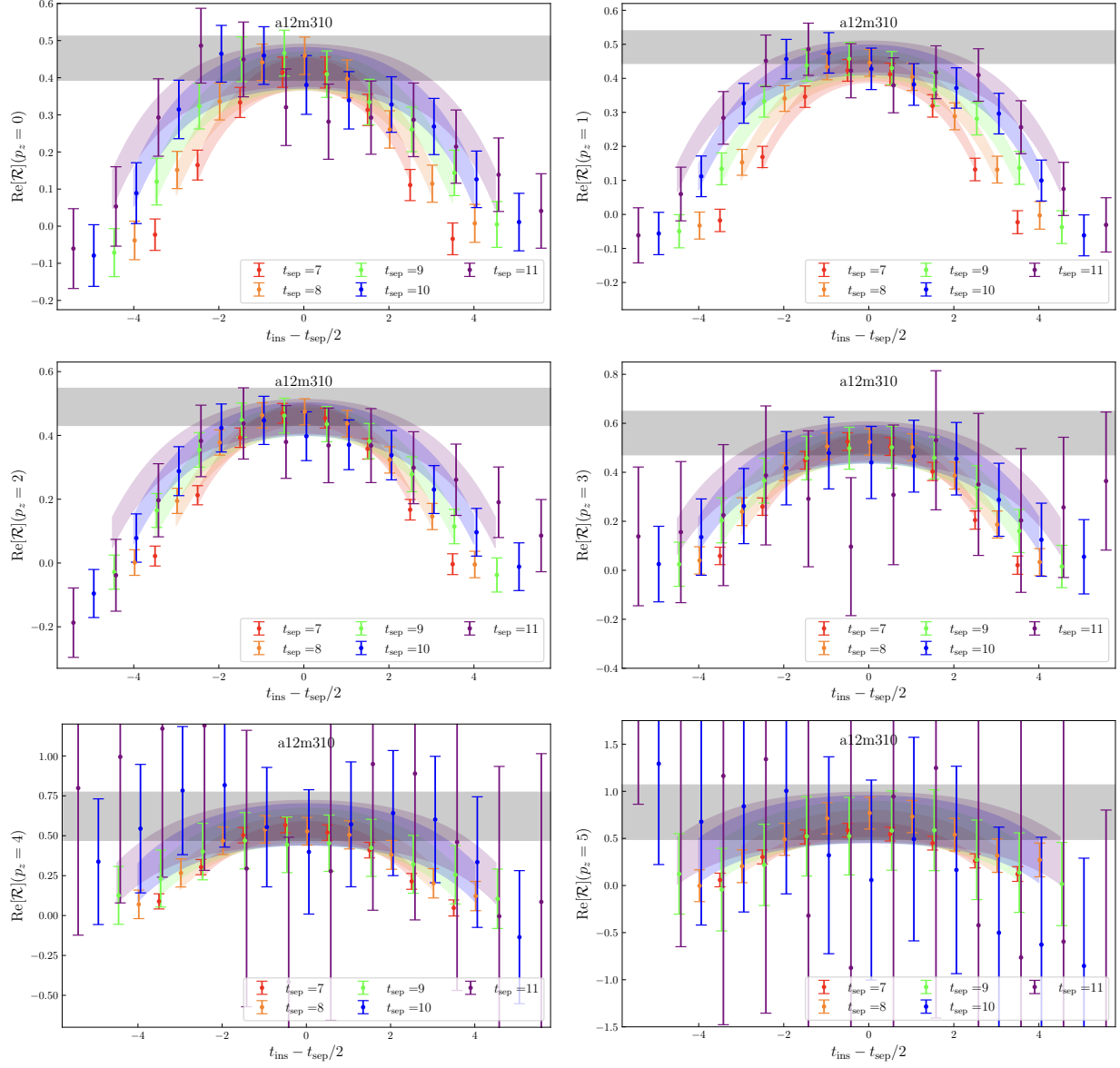


Figure 3.2: Plots of the 3pt/2pt correlator ratio defined in Eq. 3.8 vs. $t - \tau/2$ (so that the data for different τ align and can be compared with each other) for $p_z \in [0, 5] \times 2\pi/(aL)$ for the a12m310 ensemble. Note that $t = t_{\text{ins}}$ and $\tau = t_{\text{sep}}$ in the plots. Data for different t_{sep} are offset horizontally from each other so that data points that otherwise overlap can be distinguished. The gray band denotes $\langle 0|O_{g,tt}|0\rangle$. For $p_z = 4, 5 \times 2\pi/(aL)$, some of the data goes outside the bounds of the plot because the error increases with t_{sep} and with momentum.

p_z	$ A_0 ^2 \mathcal{M}_{00}$	$ A_0 A_1 \mathcal{M}_{01}$	$ A_1 ^2 \mathcal{M}_{11}$	$\langle 0 O_{g,tt} 0\rangle$	χ^2/dof
0	3.488(460)e-10	-5.950(933)e-10	1.158(741)e-8	0.453(59)	0.541(507)
1	1.320(129)e-9	-2.127(246)e-9	2.629(1409)e-8	0.492(48)	0.307(386)
2	4.146(494)e-9	-6.639(781)e-9	1.255(395)e-7	0.490(58)	0.454(401)
3	1.369(218)e-8	-2.014(275)e-8	3.196(1627)e-7	0.560(89)	0.259(252)
4	3.767(917)e-8	-4.928(963)e-8	5.387(7204)e-7	0.622(151)	0.354(360)
5	9.538(3569)e-8	-1.203(307)e-7	3.281(28207)e-7	0.778(289)	0.221(194)

Table 3.2: Fit parameters the 3pt correlator two-sim fits to Eq. 3.7 and the corresponding χ^2/dof for the a12m310 ensemble for $p_z \in [0, 5] \times 2\pi/(aL)$, $\mathcal{M}_{ij} = \langle i|O_{g,tt}|j\rangle$. Fits were performed using $\tau \in [7, 11]$. For the noisiest data (largest p_z), the error on some of the parameters is on the same order as the parameters themselves. For $p_z = 5$, the error on $|A_1|^2 \mathcal{M}_{11}$ is actually an order of magnitude larger than the parameter. $\langle 0|O_{g,tt}|0\rangle$ must be divided by a kinetic factor to convert it to $\langle x \rangle_g^{\text{bare}}$.

Chapter 4

Nonperturbative Renormalization (NPR)

4.1 Regularization-independent Momentum Subtraction (RI/MOM) Scheme

Some quantities calculated via LQCD must be renormalized in order to be compared to the same quantities calculated by other means, including other lattice calculations that use different definitions of quantities. For example, the gluon momentum fraction of the nucleon is independent of the definition of the gauge energy-momentum tensor (EMT) (e.g. clover vs. plaquette definitions) after nonperturbative renormalization (NPR) is applied to the EMT [5].

This chapter references a paper of which I am a co-author [4], and the use of first person singulars like “I” indicates that I am referring to the work that I specifically completed whereas plurals like “we” refer to the work in that paper completed mostly by the primary author (though I double-checked some of the work). We used $N_f = 2 + 1 + 1$ highly-improved staggered quarks (HISQ) [6] generated by the MILC collaboration [7]. They are the same lattice ensembles that were used in Chapter 3, and their parameters are summarized in Table 4.1.

ensemble	a09m310	a12m310	a15m310
a (fm)	0.0888(8)	0.1207(11)	0.1510(20)
$L^3 \times L_t$	$32^3 \times 96$	$24^3 \times 64$	$16^3 \times 48$
M_π^{val} (MeV)	313.1(13)	309.0(11)	319.1(31)
$M_{\eta_s}^{\text{val}}$ (MeV)	698.0(7)	684.1(6)	687.3(13)
N_{cfg}	1009	1013	900

Table 4.1: Lattice spacing a in fm, lattice size $L^3 \times L_t$, valence pion and η_s masses M_π^{val} and $M_{\eta_s}^{\text{val}}$ in MeV, and number of configurations N_{cfg} for the lattice ensembles analyzed in Chapter 4. Data taken from [4].

The gauge links undergo 5 steps of hypercubic smearing (5-HYP) [8] to reduce statistical uncertainties [9]. The gluon fields are gauge-fixed in the Landau gauge by calculating them from the link variables $U_\mu(x)$ as

$$A_\mu(p) = a^4 \sum_{x \in \Lambda} e^{ip \cdot \left(x + \frac{1}{2} \hat{\mu}\right)} \left[\frac{U_\mu(x) - U_\mu^\dagger(x)}{2ig_0 a} \right]_{\text{traceless}}, \quad (4.1)$$

where the trace (over color) has been subtracted from the term in brackets.

In my particular work, I calculated the necessary renormalization factors for converting the bare gluon momentum fraction of the nucleon, denoted as $\langle x \rangle_g$ (where x is the momentum fraction), calculated from LQCD to the same quantity in the modified minimal subtraction scheme $\overline{\text{MS}}$ (MS-bar) using a regularization-independent momentum-subtraction (RI/MOM) scheme. The gluon momentum fraction is equal to the overlap with the ground state of the temporal component of the energy-momentum tensor (EMT), $O_{g,tt}$, after kinematic factors that arise from the normalization of the fields and the choice of projection are divided out. That is, $\langle x \rangle_g \propto \langle 0 | O_{g,tt} | 0 \rangle$, where

$$O_{g,\mu\nu} = F_{\mu\rho} F_{\nu\rho} - \frac{1}{4} g_{\mu\nu} F_{\rho\sigma} F_{\rho\sigma}, \quad (4.2)$$

where $F_{\mu\nu}$ is the gluon field strength tensor and $g_{\mu\nu}$ is the metric. Thus, renormalizing $\langle x \rangle_g$ is equivalent to renormalizing the operator O_g .

The renormalization procedure outlined here is derived in Refs. [5, 10] and also utilized in our work [4]. The renormalized gluon momentum fraction in the $\overline{\text{MS}}$ scheme can be written as

$$\langle x \rangle_g^{\overline{\text{MS}}} = Z_{O_g}^{\overline{\text{MS}}}(\mu^2, \mu_R^2) \langle x \rangle_g^{\text{bare}} = R^{\overline{\text{MS}}}(\mu^2, \mu_R^2) Z_{O_g}^{\text{RI}}(\mu_R^2) \langle x \rangle_g^{\text{bare}}, \quad (4.3)$$

where the Z 's are renormalization constants, μ and μ_R are energy scales, and $R^{\overline{\text{MS}}}(\mu, \mu_R)$ is the one-loop perturbative matching ratio given by

$$R^{\overline{\text{MS}}}(\mu^2, \mu_R^2) = 1 - \frac{g^2 N_f}{16\pi^2} \left[\frac{2}{3} \ln \left(\frac{\mu^2}{\mu_R^2} \right) + \frac{10}{9} \right] - \frac{g^2 N_c}{16\pi^2} \left(\frac{4}{3} - 2\xi + \frac{\xi^2}{4} \right). \quad (4.4)$$

In this equation, derived in Ref. [11], N_f is the number of flavors, N_c is the number of colors, $g^2 = 4\pi\alpha(\mu)$ is the coupling strength (with $\alpha(\mu)$ as the coupling constant), and ξ is the parameter from Riemann's zeta function. In this work, $N_f = 4$, $N_c = 3$, $\xi = 0$ in the Landau gauge, and $\mu = 2$ GeV. The RI/MOM renormalization constant $Z_g^{\text{RI}}(\mu_R^2)$ can be obtained from the normalization condition

$$Z_g(p^2) Z_{O_g}^{\text{RI}}(p^2) \Lambda_{O_g}^{\text{bare}}(p^2) \left(\Lambda_{O_g}^{\text{tree}}(p^2) \right)^{-1} \Big|_{p^2=\mu_R^2} = 1, \quad (4.5)$$

where $Z_g(p^2)$ is the gluon-field renormalization constant, and $\Lambda_{O_g}(p^2)$'s are amputated Green's functions for the operator O_g for gluons in the Landau gauge. In Refs. [5, 10], from this condition, it is shown that

$$\left(Z_{O_g}^{\text{RI}} \right)^{-1}(\mu_R^2) = \frac{p^2 \langle (O_{g,\mu\mu} - O_{g,\nu\nu}) \text{Tr}[A_\tau(p)A_\tau(-p)] \rangle}{2(p_\mu^2 - p_\nu^2) \langle \text{Tr}[A_\tau(p)A_\tau(-p)] \rangle} \Big|_{p^2=\mu_R^2, \tau \neq \mu \neq \nu, p_\tau=0}, \quad (4.6)$$

where there is no summation over repeated indices. The quantity $\text{Tr}[A_\mu(p)A_\nu(-p)]$ is the gluon propagator or gluon 2pt function and is also written as

$$D_{g,\mu\nu}(p) = \text{Tr}[A_\mu(p)A_\nu(-p)], \quad (4.7)$$

such that the quantity used in Eq. 4.6 is $D_{g,\tau\tau}$.

4.2 Cluster-decomposition Error Reduction (CDER)

Naïve attempts to calculate $Z_{O_g}^{\overline{\text{MS}}}$ proved difficult as a signal-to-noise ratio under 100% was obtained [5, 4]. In order to improve the signal, a technique was developed in Ref. [5] called cluster-decomposition error reduction (CDER). The motivation for this method is that the correlators decay exponentially in the distance between operator insertions (e.g. gluon fields and the EMT), so there is no point in integrating beyond the correlation length as it will only pick up noise. This is implemented by imposing cutoffs in the spatial integrals used to calculate the correlators. In this specific work, they become [4]

$$\begin{aligned} D_{g,\tau\tau} &= \langle \text{Tr}[A_\tau(p)A_\tau(-p)] \rangle \approx \left\langle \int_{|r'| < r_2} d^4 r' \int d^4 x e^{ip \cdot r'} \text{Tr}[A_\tau(x)A_\tau(x+r')] \right\rangle \\ C_3^{\text{CDER}}(p) &= \langle O_{g,\mu\nu} \text{Tr}[A_\tau(p)A_\tau(-p)] \rangle \approx \left\langle \int_{|r| < r_1} d^4 r \int_{|r'| < r_2} d^4 r' \int d^4 x e^{ip \cdot r'} \right. \\ &\quad \left. \times O_{g,\mu\nu}(x+r) \text{Tr}[A_\tau(x)A_\tau(x+r')] \right\rangle. \end{aligned} \quad (4.8)$$

In Ref. [5], they found that $r_1 \approx 0.9$ fm and $r_2 \approx 1.3$ fm reduces the uncertainty by a approximately a factor of $2V(\pi^2 r_1^2 r_2^2)$.

Although the CDER method outlined above seems robust and reliable for improving

the signal-to-noise ratio, we took a slightly different approach that was motivated by these results. Rather than using a spherical cutoff, we used a hypercubic cutoff by truncating our lattices into $16 L_c^4$ sub-lattices such that $L_c \approx 2r_1, 2r_2$. This method also increases the number of measurements that we are able to make from N_{cfg} to approximately $16N_{\text{cfg}}$ where N_{cfg} is the original number of lattice configurations.¹ The truncations were implemented by selecting a random lattice site to serve as the center of the sub-lattice. Then, we create the sub-lattice by selecting the L_c points in every dimension that surround this center. For example, if lattice site (n_1, n_2, n_3, n_4) is the randomly chosen center, then the Cartesian product

$$\prod_{\mu=1}^4 \left\{ n_\mu - \frac{L_c}{2}, n_\mu - \frac{L_c}{2} + 1, \dots, n_\mu, n_\mu + 1, \dots, \frac{L_c}{2} - 1 \right\}$$

is the set of points in the sub-lattice. For lattice with L divisible by 4, the center is not actually the true center because the L_c sites in a given dimension must be chosen such that $L_c/2$ are on one of the center and $L_c/2 - 1$ are on the other side (because the center is one of the L_c sites). However, this does not really matter; the lattice site that is randomly selected could also be chosen to be one of the corners instead. My only recommendation is that the randomly selected point have a consistent definition on each sub-lattice. On each sub-lattice, lattice quantities like $D_{g,\mu\nu}(p)$ and $F_{\mu\nu}F_{\rho\sigma}$ are calculated as they would be for the entire lattice for all combinations of spacetime indices and several p .

Our work in Ref. [4] shows that this method is successful in increasing the signal-noise ratio, and different choices of L_c produce consistent results on a given ensemble. This was demonstrated by calculating $\left(Z_{O_g}^{\overline{\text{MS}}}\right)^{-1}(\mu^2, \mu_R^2)$ using the full lattice and using different truncations and plotting the results to show that the truncated lattices produce much smaller

¹It's approximate because some truncations could not be transferred from the cluster to my local machine.

error. We decided on $L_c = L/2$ where L is the spatial extent of the original lattice, which corresponds to $aL_c \in [1.2, 1.4]$ fm and $r_1 \approx 0.7$ fm, consistent with the choices of cutoff in Ref. [5]. This information is summarized in Table 4.2.

ensemble	a09m310	a12m310	a15m310
L	32	24	16
L_c	16	12	8
aL_c (fm)	1.44	1.44	1.2
N_{cfg}	347	409	900
N_{meas}	5552	6543	14,388

Table 4.2: The original spatial extent L , truncated lattice size $L_c = L/2$, physical size aL_c of each lattice, number of configurations N_{cfg} , and number of measurements $N_{\text{meas}} \approx 16N_{\text{cfg}}$.

4.3 Renormalized Gluon Momentum Fraction

$\left(Z_{O_g}^{\text{RI}}\right)^{-1}(\mu_R^2)$ is calculated according to Eq. 4.6. Different combinations of τ , μ , and ν satisfy the condition given in the equation. In this work, we only used combinations such that $\mu = (\tau \bmod 4) + 1$ and $\nu = (\mu \bmod 4) + 1$. Thus, each value of $\left(Z_{O_g}^{\text{RI}}\right)^{-1}(\mu_R^2)$ used for future calculations is the average of four different values that correspond to the four different possible choices of τ (one for each spacetime dimension). Additionally, when calculating $\langle(O_{g,\mu\mu} - O_{g,\nu\nu}) \text{Tr}[A_\tau(p)A_\tau(-p)]\rangle$, we subtracted the means of $(O_{g,\mu\mu} - O_{g,\nu\nu})$ and $\text{Tr}[A_\tau(p)A_\tau(-p)]$ from themselves before multiplying them together. This is done because the means of each quantity are supposed to be 0 anyway, so it improves the quality of the end result.

In order to calculate the renormalized gluon momentum fraction $\langle x \rangle_g$, which is calculated for 0 momentum transfer in the 3pt correlator, the renormalization constant $Z_{O_g}^{\overline{\text{MS}}}(\mu^2, p^2) = R^{\overline{\text{MS}}}(\mu^2, p^2) Z_{O_g}^{\text{RI}}(p^2)$ must be extrapolated (μ to $p^2 = 0$). The calculated $\left(Z_{O_g}^{\text{RI}}\right)^{-1}(p^2)$ are

divided by $R^{\overline{\text{MS}}}(\mu^2, p^2)$ calculated by Eq. 4.4 to obtain $(Z_{O_g}^{\overline{\text{MS}}})^{-1}(\mu^2, p^2)$. Because of the relatively small dependence of $(Z_{O_g}^{\overline{\text{MS}}}(\mu^2, p^2))^{-1}$ on p^2 , we fit the data to

$$(Z_{O_g}^{\overline{\text{MS}}})^{-1}(\mu^2, p^2) = (Z_{O_g}^{\overline{\text{MS}}})^{-1} + c_1 p^2 + c_2 p^4, \quad (4.9)$$

where $(Z_{O_g}^{\overline{\text{MS}}})^{-1}$ is the reciprocal of the renormalization constant at $p^2 = 0$. This functional form is chosen because its constituents contain p^2 , as seen in Eqs. 4.4–4.6. Thus, any Taylor expansions will only contain even powers of $|p|$. The relatively weak dependence of the data points on p^2 , as seen in Fig. 4.1, justifies fitting only up to quadratic order in p^2 . It should be noted that previous works only fitted to a constant [12] or to linear order in p^2 [10].²

The smallest p used for each fit are 2.4, 2.0, and 1.5 GeV for a15m310, a12m310, and a09m310, respectively, just as PNDME in their study on the same mixed-action [12] as in this study, in order to avoid non-perturbative effects. As for the upper bound of the fitting range, it is shown in our previous work [4] that $(Z_{O_g}^{\overline{\text{MS}}})^{-1}$ is mostly consistent for different choices of the upper bound provided that the upper p^2 is sufficiently large. Because of this, I did not impose an upper bound. The results are shown in Fig. 4.1 and Table 4.3.

ensemble	a09m310	a12m310	a15m310
$(Z_{O_g}^{\overline{\text{MS}}})^{-1}$	1.562(69)	1.403(45)	0.998(20)

Table 4.3: $\overline{\text{MS}}$ renormalization constants $(Z_{O_g}^{\overline{\text{MS}}})^{-1}$ calculated with the RI/MOM scheme by fitting our calculated data points to Eq. 4.9. These values correspond to the reconstructed fit band range at $p^2 = 0$ in Fig. 4.1.

²Other works [5, 10] used the dimensionless $(ap)^2$ as the expansion parameter, but this does not change the results since the 0th-order term is unaffected and the a^{2n} can be absorbed into the fitting parameters c_n .

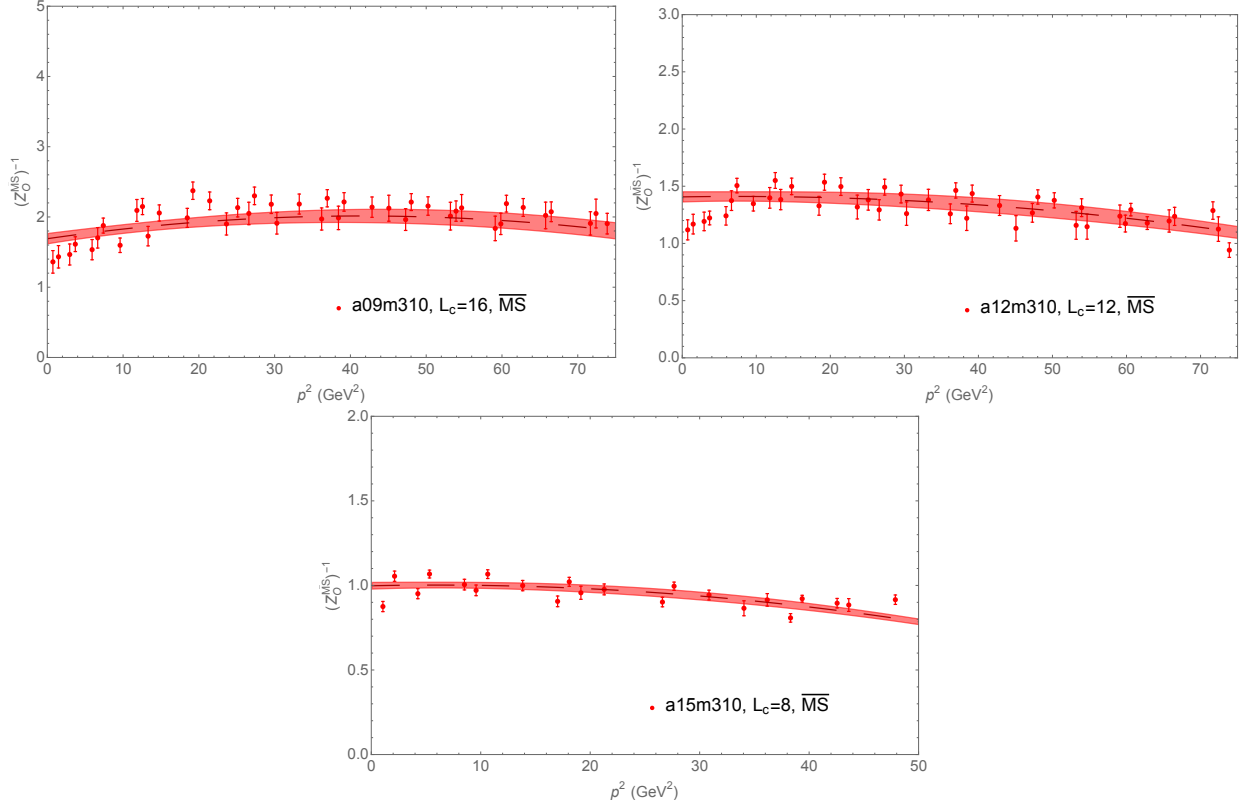


Figure 4.1: $\left(Z_{O_g}^{\overline{\text{MS}}}\right)^{-1}(\mu^2, p^2)$ vs. p^2 for the a09m310 (upper left), a12m310 (upper right), and a15m310 (lower) ensembles. The minimum p^2 for each fit are 2.4^2 , 2^2 , and 1.5^2 GeV^2 for a09m310, a12m310, and a15m310, respectively, as in Ref. [12]. Thus, the reconstructed fit bands do not pass through data points for the smallest p^2 for a09m310 and a12m310. The data shows fairly weak dependence on p^2 , which justifies a fit that is quadratic in p^2 .

4.4 NPR Calculation Workflow

I will now explain the sequence of programs and calculations required to turn lattice data to calculated renormalization constants in the RI/MOM scheme. In particular, I will explain how the relevant equations that are stated earlier in this chapter were practically implemented to calculate necessary quantities. There are two major sections of the code. The first is a **Chroma**³ code that must be run on a supercomputer cluster. The second is a **Mathematica**⁴ notebook that can be run on any modern personal computer with a multi-core CPU, although around 100 GB of available disk space is recommended to store the necessary input files. The workflow for each of these steps is outlined in the flowcharts in Figs. 4.2 and 4.3.

4.4.1 Chroma

All of the following calculations were done with the **Chroma** software library running on the Fermilab National Accelerator Laboratory (FNAL) lattice QCD supercomputer cluster, abbreviated here as FNAL. The process of calculating the NPR constant begins with using a lattice gauge configuration as input. **Chroma** also requires XML files as input that specify what is to be calculated. One of the elements in the XML file is the path of the lattice file. All of the XML files are generated by **Perl** scripts that require only a couple of command line arguments to specify either the lattice location and/or the output location (if this particular step outputs another lattice file). They print to console, so the output must be redirected into an XML file. Each time the **Chroma** executable is run, it sends output to `stdout`, but it is not all necessary for future calculations.

³<https://jeffersonlab.github.io/chroma/>

⁴<https://www.wolfram.com/mathematica/>

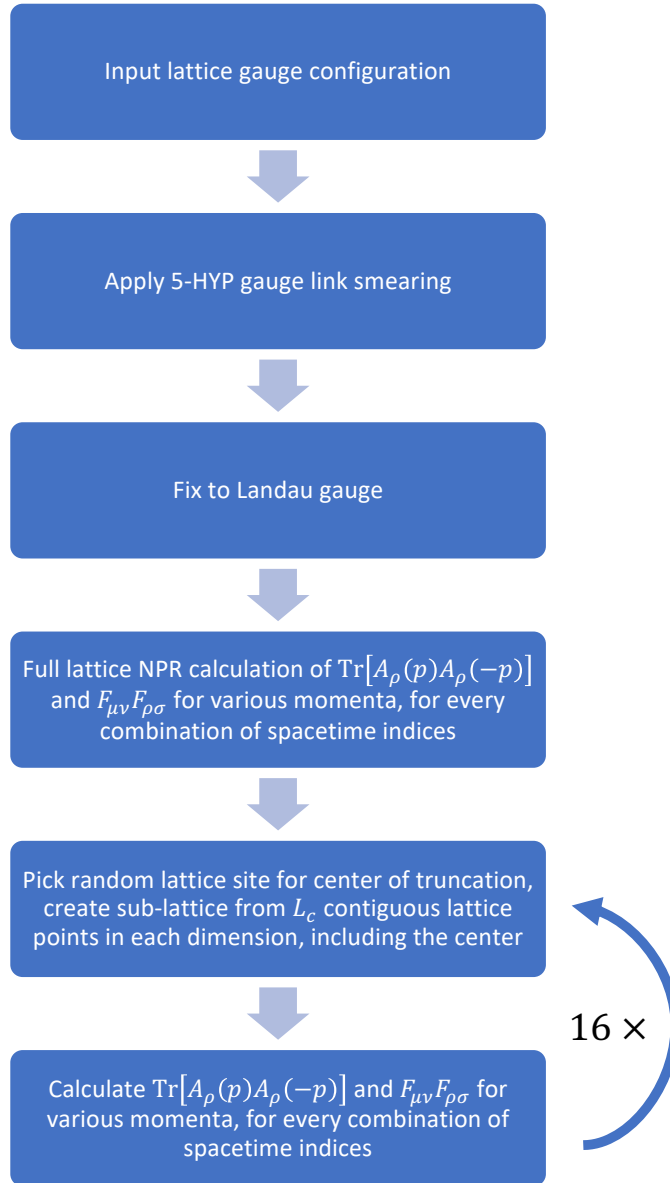


Figure 4.2: Outline of the steps for running the first major section of the NPR code, i.e. the **Chroma** section. We repeated the truncation steps (last two steps) 16 times for each lattice configuration.

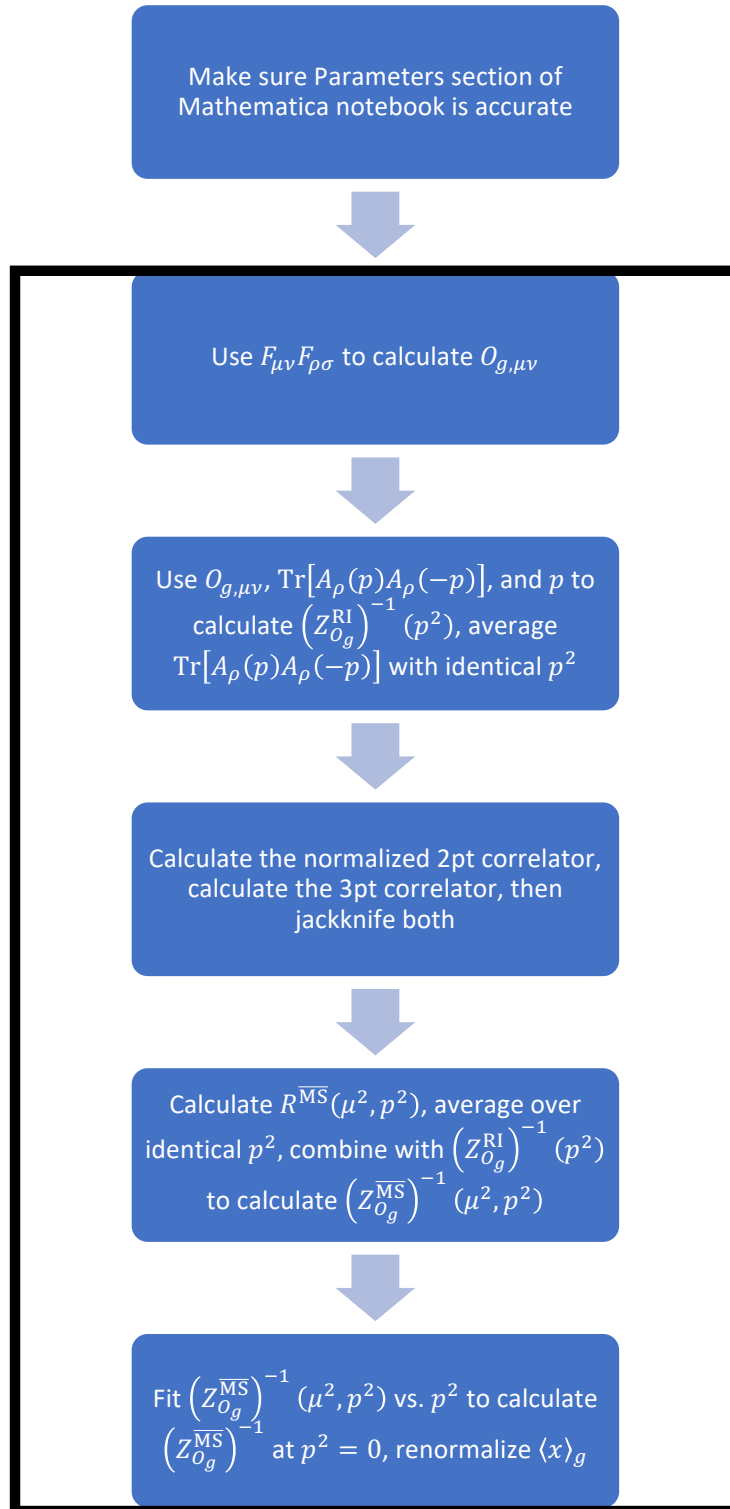


Figure 4.3: Outline of the steps for running the second major section of the NPR code, i.e. the **Mathematica** section. I organized the notebook such that after the necessary parameters are entered, the rest of the notebook can be run at once and treated as a black box. These parts of the code are denoted by the black rectangle.

The FNAL cluster uses `Slurm` as its job manager, so our work was completed by submitting `sbatch` scripts. There are a few variables in the script that need to be set first. They are listed below:

- `INDIR`: The submission directory for the script containing the `Perl` scripts and directories that will contain the output XML files. Works best if set to `SLURM.SUBMIT.DIR`.
- `OUTDIR`: Set equal to `INDIR`.
- `HYP1LOC`: Directory containing the input lattice files. These files already have one step of hypercubic smearing (1-HYP) applied to them, so we need to apply four more.
- `HYP5LOC`: Directory that will contain the output lattices that have 5-HYP smearing applied.
- `LATFILENAME`: The portion of the lattice file names up to and not including the first dot, e.g. `148144f211b672m0048m024m286a` if the lattice file is
`148144f211b672m0048m024m286a.hyp.2100`
- `Ls`: Integer spatial extent of the lattice.
- `Lt`: Integer temporal extent of the lattice.
- `exe`: Path to `Chroma` executable.
- `exe1`: Path to lattice truncation part 1 executable.
- `exe2`: Path to lattice truncation part 2 executable.
- `trunc_out`: Directory that will contain the truncated lattice files.
- `OMP_NUM_THREADS`: Number of threads used for thread parallelism. Should be set to 1.

- **GEOM**: String of four integers, each separated by a space. The four integers must multiply to the number of cores/tasks requested. The first three should ideally be identical and must divide the spatial extent of the lattice. The last integers must divide the temporal extent. For example, if 512 tasks are requested for a $48^3 \times 144$ lattice, we could have `GEOM="4 4 4 8"`. These numbers must also evenly divide the L_c^4 sub-lattices.

In addition to initializing environment variables, certain directories must be created before the script can be run. They are:

- **HYP5LOC**: The user must manually create the directory whose path is the value of this variable in advance.
- **trunc_out**: The user must manually create the directory whose path is the value of this variable in advance.
- `INDIR/xmls`
- `INDIR/xmls.GTG`
- For each choice of truncated size L_c , there must be a folder `INDIR/xmls.LX.GT` where X is replaced by the truncation size with no leading zeroes. For example, $L_c = 8$ and $L_c = 12$ require `INDIR/xmls.L8.GT` and `INDIR/xmls.L12.GT`, respectively.

The first step that we perform is applying the 5-HYP smearing to the gauge links. This is done by running the `HYP.pl` script where the first argument is the path to the lattice gauge configuration (i.e. the ones produced by the MILC collaboration) and the second argument is the path where the output lattice file that has been smeared should be created. Run `exe` with the XML created by `HYP.pl` as the input.

The second step is applying the gauge-fixing. This is done by running the `GF.pl` script where the first argument is the path to the newly-created smeared lattice from the previous step and the second argument is the path where the output lattice file that has been gauge-fixed will be created. Run `exe` with the XML created by `GF.pl`.

Third, the full lattice NPR calculation is performed. This is done by running the `NPR.gluon.gf.pl` script where the first argument is the path to the newly-created gauge-fixed lattice file from the previous step and the second argument is the maximum p^2 in integer units (100 in our work). Run `exe` with the XML created by `NPR.gluon.gf.pl`. The details of how this section of the code works and some of the difficulties with this step will be explained later. This step outputs both $F_{\mu\nu}F_{\rho\sigma}$ and $D_{g,\mu\nu}(p)$ for momenta up to the square root of the second argument to the `NPR.gluon.gf.pl`. For, $F_{\mu\nu}F_{\rho\sigma}$, only the entries with zero momentum are needed. The data is organized as such. For, $F_{\mu\nu}F_{\rho\sigma}$ a line of data is formatted as:

$$\text{FF } p \quad \mu \quad \nu \quad \rho \quad \sigma \quad \text{Re} [F_{\mu\nu}F_{\rho\sigma}] \quad \text{Im} [F_{\mu\nu}F_{\rho\sigma}],$$

and a line of $D_{g,\mu\nu}$ data is formatted as:

$$\text{G2ptp } \mu \quad \nu \quad p_x \quad p_y \quad p_z \quad p_t \quad \text{Re} [D_{g,\mu\nu}] \quad \text{Im} [D_{g,\mu\nu}].$$

Next, the lattice data is restructured in preparation for truncation. This is done by running the `trun_xmlpart1.pl` script where the first argument is the gauge-fixed lattice from before and the second argument is the path where the output lattice file will be generated. Run `exe1` with the XML created by `trun_xmlpart1.pl`. Then, the lattice is actually truncated. The `sbatch` script loops over each desired L_c . Each truncation is performed 16 times at a random part of the lattice each time. The scripts for this section are `trun_xmlpart2_LX.pl`

where X is the value of L_c . They require the following six command line arguments in this order: the path to the restructured lattice file that was just created, the path to the restructured lattice file up to and excluding `.vec` (this is used to create the output lattices that have been truncated), the x -coordinate of the truncation center, the y -coordinate of the truncation center, the z -coordinate of the truncation center, the t -coordinate of the truncation center. Each of the 16 randomly-chosen center coordinates produces a different XML file. Run `exe2` once with each XML file.

Finally, the NPR calculation on the truncated lattices is performed. The `sbatch` script searches for the truncated lattice files of a given L_c and loops over them. Then the script `NPR.gluon.LX.p1` where X is the value of L_c is run for each lattice file where the first argument is the path to the truncated lattice and the second argument is the maximum p^2 (100 in our work). Then, run `exe` with these XML files that were created. As with the full lattice calculation, the output sent to `stdout` has data that is needed for the next steps. Place the lines beginning with `FF` with zero momentum in files named `FF_CFG_TRUNC_LC.txt` and the lines of data that begin with `G2ptp` in files named `G2pt_CFG_TRUNC_LC.txt`. The rest of the lines should not be added to these files. Also, although this step outputs $\text{Tr}[A_\mu(p)A_\nu(-p)]$, recall that only the entries with $\mu = \nu \equiv \tau$ are needed. This will be taken care of later. These files are required for the `Mathematica` code that will be run next.

4.4.1.1 Implementation of the NPR Calculation

The NPR calculation itself has a few different steps to obtain $F_{\mu\nu}F_{\rho\sigma}$ and $D_{g,\mu\nu}(p)$ from the gauge-fixed or truncated input lattices. Because it is the most complicated of the above steps, the source code deserves further explanation.

4.4.2 Mathematica

Once the `Chroma` step is completed, its output is used in the `Mathematica` notebook. The most important requirement is to set everything correctly in the “Parameters” section at the very beginning of the notebook. This includes lattice parameters, input directories that contain the required $F_{\mu\nu}F_{\rho\sigma}$ and $\text{Tr}[A_\mu(p)A_\nu(-p)]$, output directories, the matching scale μ (used to calculate the previously-mentioned perturbative matching ratio), and a few other parameters that are explained in the notebook. The user must also create a file containing a list of the lattice configuration numbers that were used and specify which truncations in a given configuration are not usable, if any (this feature was implemented after I found files that were empty or incomplete). Other lines do not need to be modified by the user, such as certain variables that check whether the files created by the notebook already exist. The subsequent sections that perform calculations will not run if their output already exists. This is useful if, for example, one only has already run the notebook but wants to use the output to make plots at the end. As long as this section is modified correctly, the rest of the notebook can be run at once and treated as a black box until the plots at the end of the notebook are created. Also, this section contains a variable with many values of μ in GeV and the corresponding value of the running coupling constant $\alpha(\mu)$ hard-coded, and an interpolation is performed so that this quantity can be used to calculate $g^2(\mu) = 4\pi\alpha(\mu)$. This is needed to calculate $R^{\overline{\text{MS}}}(\mu^2, \mu_R^2)$ (Eq. 4.4) later on.

The next section of the notebook calculates the gluon EMT $O_{g,\mu\mu}$ (only the diagonals). The $O_{g,\mu\mu} - O_{g,\nu\nu}$ in Eq. 4.6 term means that the $F_{\rho\sigma}F_{\rho\sigma}$ in Eq. 4.2 term does not need to be calculated because it cancels when diagonal terms of O_g are subtracted as in Eq. 4.6. Thus, the notebook parses through the files containing $F_{\mu\nu}F_{\rho\sigma}$ to find entries where $\mu = \rho$

and $\nu = \sigma$, and then it calculates O_g . Only the real part of $F_{\mu\nu}F_{\rho\sigma}$ is needed. Also, the calculated O_g needs to be divided by 2 because of how $F_{\rho\sigma}F_{\rho\sigma}$ was calculated in **Chroma**.

The next section of the notebook calculates the gluon propagator or 2pt function $D_{g,\tau\tau}(p)$. This section requires the most runtime by far because the files containing the $D_{g,\mu\nu}(p)$ data have over 300,000 lines. Thus, the notebook is bottlenecked by how quickly these files can be read rather than the calculations. However, only a few of these lines are needed for calculations, and the line numbers are the same for every file. To improve efficiency, the notebook first parses through the first file for the lines that have $\mu = \nu \equiv \tau$ and $p_\tau = 0$, as required by Eq. 4.6, but also $p_{[(\mu+1) \bmod 4]+1} = 0$. Since we used $\mu = (\tau \bmod 4) + 1$ and $\nu = (\mu \bmod 4) + 1$, where the indices correspond to Eq. 4.6, this corresponds to $p_\nu = 0$. This is consistent with the derivation in Ref. [5]. For example, if $\tau = t$ (index 4), then $p_y = 0$ is required. These line numbers are stored in a list. Then, each file containing $D_{g,\mu\nu}(p)$ is parsed and the gluon 2pt function is calculated. In addition to the 2pt function, a quantity called the normalized 2pt function is also calculated, equal to

$$-\frac{2p_\mu^2 D_{g,\tau\tau}(p)}{p^2}, \quad (4.10)$$

where the additional terms correspond to the momenta in Eq. 4.6. The negative sign is required to make the renormalization constant positive and probably comes from how $D_{g,\mu\nu}(p)$ was calculated in **Chroma**.

In this process, the momentum 4-vector is mapped to the raw and normalized 2pt functions. Then, another map maps the p^2 in integer units to the 2pt function by averaging over all values with the same p^2 . The mapping is done in these two separate steps because there are multiple definitions used for the momentum. In particular, Refs. [5, 10] reference

a definition motivated by the poles of the lattice propagator, given by

$$a\tilde{p}_\mu = 2 \sin\left(\frac{ap_\mu}{2}\right) = 2 \sin\left(\frac{\pi n_\mu}{L_\mu}\right), \quad (4.11)$$

where the second equality uses $p_\mu = 2\pi n_\mu/(aL_\mu)$ where $n_\mu \in \{0, 1, \dots, L_\mu - 1\}$. Both this definition and the standard Euclidean definition of the square of the momentum magnitude are mapped to the 2pt function although analysis primary focuses on the latter in our work. For this former, the map maps $(a\hat{p})^2$ in exact symbolic form to the 2pt function. All of these maps are saved as well as a map of the integer p^2 to the p^2 in physical units of GeV^2 (Euclidean definition).

After the gluon 2pt propagator has been calculated and averaged over identical momenta, the next section of the notebook calculates the quantity $(O_{g,\mu\mu} - O_{g,\nu\nu}) D_{g,\tau\tau}(p)$. This quantity is called the gluon 3pt function. First, the $O_{g,\mu\mu}$ calculated from the previous section are used to calculate the required differences $O_{g\mu\mu} - O_{g\nu\nu}$. Since each τ only uses $\mu = (\tau \bmod 4) + 1$ and $\nu = (\mu \bmod 4) + 1$, for each μ , only one value of ν is required to perform calculations. Thus, the data is stored in a **Table** as

$$\{O_{g,yy} - O_{g,zz}, O_{g,zz} - O_{g,tt}, O_{g,tt} - O_{g,xx}, O_{g,x} - O_{g,yy}\}.$$

This means that the index of this list is τ , e.g. the first entry corresponds to $\tau = x$ (index 1) such that $O_{g,yy} - O_{g,zz}$ is needed. The operator is combined with the 2pt function as

$$\left\langle \left[(O_{g,\mu\mu} - O_{g,\nu\nu}) - \overline{(O_{g,\mu\mu} - O_{g,\nu\nu})} \right] \left[D_{g,\tau\tau}(p) - \overline{D_{g,\tau\tau}(p)} \right] \right\rangle,$$

where the overline denotes the mean over all configurations. This calculation subtracts the

mean of each quantity from itself as described earlier. Note that the non-normalized 2pt function is used in this calculation. Once the 3pt function has been calculated, this quantity is divided by the normalized 2pt function. The results are stored in maps that map p^2 to the ratios, one map for each momentum definition.

The last section of the notebook begins by averaging the ratios from the previous section over τ as the previous calculation produces a different value for each spacetime coordinate. At this point, $\left(Z_{Og}^{\text{RI}}\right)^{-1}(p^2)$ has been calculated. Then, $\left(Z_{Og}^{\text{MS}}\right)^{-1}(\mu^2 = 4 \text{ GeV}^2, p^2)$ is finally calculated. First, $R^{\text{MS}}(\mu^2 = 4 \text{ GeV}^2, p^2)$ is calculated using the interpolated $\alpha(\mu)$ in the “Parameters” section at the beginning of the notebook. This is combined with $\left(Z_{Og}^{\text{RI}}\right)^{-1}(p^2)$ to calculate $\left(Z_{Og}^{\text{MS}}\right)^{-1}(\mu^2 = 4 \text{ GeV}^2, p^2)$ as

$$\left(Z_{Og}^{\text{MS}}\right)^{-1}(\mu^2 = 4 \text{ GeV}^2, p^2) = \left(Z_{Og}^{\text{RI}}\right)^{-1}(p^2) / R^{\text{MS}}(\mu^2 = 4 \text{ GeV}^2, p^2). \quad (4.12)$$

Then, the data points are fitted to Eq. 4.9 using data points that satisfy $p^2 > \text{p2fitmin}$ defined in the “Parameters” section. This section also makes a plot of the data points and the reconstructed fit band on separate plots. To combine them, use the `Show` function. This can be done by copying each image and pasting them as the arguments of `Show` or by saving each plot as a variable and using those variables as the arguments. Separate plots are also produced for the alternate definition of momentum in Eq. 4.11.

The plots in Fig. 4.1 were produced using notebooks that were written as described in this subsection. My work involved improving the readability and efficiency of the code, adding additional comments, double-checking calculations and formulas, and speeding up the code. I improved efficiency and runtime in various ways. I utilized more efficient data structures for the required information that we needed to store (namely maps, implemented

as the `Association` data type in `Mathematica`). This was sensible compared to the list, which functions as a map but with keys restricted to sequential integers, because the p^2 in integer units are not necessarily sequential and not necessarily in ascending order. Thus, the map also kept the data ordered in terms of ascending momentum. I also implemented the methods for parsing text files by using the fact that the needed line numbers are the same for each type of object. This improved the runtime of the notebooks from the order of days to the order of hours. In addition, the modularity of the code allows for one to make additions or modifications, particularly in the last section where the plots are produced.

Chapter 5

Electromagnetic Form Factors

PENDING.

Chapter 6

Conclusion

Lattice QCD provides an method for theoretical calculations of phenomenological parameters and observables. PENDING.

REFERENCES

- [1] Karen McNulty Walsh. Physicists zoom in on gluons' contribution to proton spin, Feb 2016.
- [2] Christof Gattringer and Christian B. Lang. *Quantum Chromodynamics on the Lattice: An Introductory Presentation*. Lecture Notes in Physics. Springer, 2010.
- [3] B.A. Berg. *Markov Chain Monte Carlo Simulations and Their Statistical Analysis: With Web-based Fortran Code*. World Scientific, 2004.
- [4] Zhouyou Fan, Huey-Wen Lin, and Matthew Zeilbeck. Nonperturbatively renormalized nucleon gluon momentum fraction in the continuum limit of $N_f = 2 + 1 + 1$ lattice qcd. *Phys. Rev. D*, 107:034505, Feb 2023.
- [5] Yi-Bo Yang, Ming Gong, Jian Liang, Huey-Wen Lin, Keh-Fei Liu, Dimitra Pefkou, and Phiala Shanahan. Nonperturbatively renormalized glue momentum fraction at the physical pion mass from lattice qcd. *Phys. Rev. D*, 98:074506, Oct 2018.
- [6] E. Follana, Q. Mason, C. Davies, K. Hornbostel, G. P. Lepage, J. Shigemitsu, H. Trotter, and K. Wong. Highly improved staggered quarks on the lattice with applications to charm physics. *Phys. Rev. D*, 75:054502, Mar 2007.
- [7] A. Bazavov, C. Bernard, J. Komijani, C. DeTar, L. Levkova, W. Freeman, Steven Gottlieb, Ran Zhou, U. M. Heller, J. E. Hetrick, J. Laiho, J. Osborn, R. L. Sugar, D. Toussaint, and R. S. Van de Water. Lattice qcd ensembles with four flavors of highly improved staggered quarks. *Phys. Rev. D*, 87:054505, Mar 2013.
- [8] Anna Hasenfratz and Francesco Knechtli. Flavor symmetry and the static potential with hypercubic blocking. *Phys. Rev. D*, 64:034504, Jul 2001.
- [9] Zhou-You Fan, Yi-Bo Yang, Adam Anthony, Huey-Wen Lin, and Keh-Fei Liu. Gluon quasi-parton-distribution functions from lattice qcd. *Phys. Rev. Lett.*, 121:242001, Dec 2018.
- [10] P. E. Shanahan and W. Detmold. Gluon gravitational form factors of the nucleon and the pion from lattice qcd. *Phys. Rev. D*, 99:014511, Jan 2019.
- [11] Yi-Bo Yang, Michael Glatzmaier, Keh-Fei Liu, and Yong Zhao. The 1-loop correction of the qcd energy momentum tensor with the overlap fermion and hyp smeared iwasaki gluon, 2016.

- [12] Santanu Mondal, Rajan Gupta, Sungwoo Park, Boram Yoon, Tanmoy Bhattacharya, and Huey-Wen Lin. Moments of nucleon isovector structure functions in $2+1+1$ -flavor qcd. *Phys. Rev. D*, 102:054512, Sep 2020.